



LUND
UNIVERSITY

Film formation of mixed-halide perovskites for PSCs

Author: Lina Ekstedt tfy12lek@student.lu.se

PHYM01

Master's Thesis (30 credits ECTS)

May 2021

Supervisor: Eva Unger

Assisting Supervisors: Carolin Rehermann and Gopinath Paramasivam

Examiner: Magnus Borgström

Abstract

Over the last few years there has been a steady increase in interest in the exploration of perovskite materials within photovoltaic research. This can to a large extent be attributed to the incredible pace at which solar cells based on perovskites have improved in efficiency during the same time period. Perovskite solar cells (SCs) are not only an alternative to today's market leading silicon based devices, but can also be a complement and improve efficiency by being used together with silicon in a tandem configuration. For mixed halide perovskites that can be used for these types of applications, fundamental knowledge about the film formation process is still insufficient to overcome some of the challenges faced. A more detailed understanding of the mechanisms, and of important conditions for film formation can help to improve the quality of the films and the performance and stability of the solar cells, which is important in order to develop market-ready solar cell devices.

This project focused on the film formation process of mixed halide perovskites and on some of the parameters affecting the film formation conditions. The $\text{MAPb}(\text{I}_x, \text{Br}_{1-x})_3$ perovskite series with different Br/I ratios was studied in-situ during spin coating of the film using an optical tracking device. Together with the subsequent use of SEM imaging, the resulting film morphology could be revealed. How antisolvent treatment conditions during spin coating affect the crystallization process and resulting film was investigated as well as how this translates to device level and the performance of the solar cells. Further, the effects on film quality and device performance when adding an alkali salt as an interface modifier (IM) in between the SnO_2 electron transport layer and the perovskite film were studied, as this has been shown to improve device performance when using other perovskite ionic compositions. [1] We found that antisolvent treatment was beneficial for formation of closed films with a smooth surface and that the timing of the antisolvent drop seemed to have a slight effect on the resulting film quality as well as on device performance. Resulting film morphology can not be directly translated from tests on glass substrates to device level as we could see that films that were spin coated on a layer of SnO_2 differed in morphology to those spin coated directly on a glass surface, and the improvement in film quality using antisolvent treatment became less apparent in these samples. Further, we found that devices in which KNO_3 was included as an IM generally had less holes in the perovskite film at the interface and the V_{OC} was improved. The effect of the IM seemed to depend on halide ratio of the perovskite as improvements in overall device performance could only be observed for the pure iodide perovskite.

Keywords: *Mixed Halide Perovskites, Perovskite Solar Cells, Bandgap Tuning, In-situ Spectroscopy, Antisolvent, Interface Modifier.*

Acknowledgements

I owe my warmest thanks to many people who were involved in my master's thesis project. I first want to thank my main supervisor Eva Unger who has supported me with ideas, planning, structure and feedback as well as the opportunity to begin my thesis work by participating at Quantsol summer school of Photovoltaics and later to come to Helmholtz-Zentrum Berlin to do most of the experiments for my thesis. I want to thank Florian Ruske at HZB who helped me to find and get in contact with Eva in the first place. A special thanks to my two main lab supervisors at HZB, Carolin Rehermann and Gopinath Paramasivam, both of which have put countless of hours of work to lead, support and often perform the experiments for my thesis project. They have additionally supported with administrative work for my visit at HZB, with ideas and knowledge for the analysis of the data and provided great company in success and failure at the lab, thank you both for a great visit at HZB.

I also want to thank the following people for additional lab supervising for my project: Janardan Dagar at HZB as well as Klara Suchan and Michael Winters at Lund University. In addition to the mentioned people, I want to thank the rest of the staff at HZB whom I had the privilege to encounter during my visit and who provided advice, guidance and practical help whenever needed. Many thanks for support and advice to my examiner Magnus Borgström and to Fanny Baumann who's simultaneous thesis project was the closest to a sister project to my own. Lastly, I would like to thank my partner for being the best possible home office mate and supporter throughout the whole period of my thesis work.

Contents

1	Introduction	7
1.1	Photovoltaics and perovskites	7
1.1.1	PV basics	7
1.1.2	Perovskite basics	7
1.2	Research Problem	9
1.3	Aim	9
2	Theory	10
2.1	Bandgap tuning and wide-bandgap perovskites	10
2.1.1	Bandgap tunability and tandem application	10
2.1.2	How to tune a bandgap	11
2.1.3	Challenges for wide-bandgap PSCs	11
2.2	Film formation process of mixed halide perovskites	13
2.3	The role of antisolvent in film formation	14
2.4	Interface modifiers	15
3	Methods	17
3.1	Project outline	17
3.1.1	Learning and preparing characterization setups	17
3.1.2	Perovskite film formation	17
3.1.3	Fabrication of solar cells	18
3.1.4	Characterization of solar cells at Lund University	18
3.2	Fabrication methods	18
3.2.1	Fabrication of perovskite films	19
3.2.2	Device architecture	20
3.2.3	Device fabrication	21
3.3	Characterization techniques	22
3.3.1	In-situ UV-vis	22
3.3.2	Scanning electron microscopy (SEM)	24
3.3.3	Current-Voltage analysis (JV)	24
3.3.4	Data analysis	26
4	Results and discussion	27
4.1	Antisolvent treatment in film formation	27
4.1.1	Film formation	27
4.1.2	Antisolvent drip timing on device performance	33
4.2	Device behaviour for varying halide compositions	36
4.3	Interface modifiers	38

4.3.1	Film quality (SEM)	39
4.3.2	Device performance	41
4.4	Discussion on methods	44
5	Conclusions	45
5.1	Empirical observations	45
5.2	Future prospects	47

Acronyms

AM1.5G Global standard spectrum, **AS** Antisolvent, **EQE** External Quantum Efficiency, **ETL** Electron Transporting Layer, **eV** Electron Volt, **FF** Fill Factor, **HI** Hysteresis Index, **HTL** Hole Transporting Layer, **HZB** Helmholtz-Zentrum Berlin, **IM** Interface Modifier, **J_{SC}** Short Circuit Current Density, **JV** Current density-Voltage, **LU** Lund University, **MPP** Maximum Power Point, **n-i-p** solar cell structure with p-type contact as front contact, **OB** Optical Batch (within project), **PCE** Power Conversion Efficiency, **PL** Photoluminescence, **PSC** Perovskite Solar Cell, **PV** Photovoltaic, **rpm** Revolutions per minute, **SC** Solar Cell, **SCB** Solar Cell Batch (within project), **SEM** Scanning Electron Microscopy, **SI** Supporting Information, **SPV** Surface Photovoltage, **UV-vis** Ultraviolet-visual spectrum, **V_{OC}** Open Circuit Voltage, **XRD** X-ray Diffraction, **X_{sol}** Iodide ratio in perovskite precursor solution.

Chemical Compounds

Au Gold, **Br** Bromide, **CaTiO_3** Calcium Titanate, **Cs** Cesium, **DMF** Dimethylformamide, **DMSO** Dimethyl Sulfoxide, **EtAc** Ethyl Acetate, **FA** Formamidinium, **I** Iodide, **ITO** Indium Tin Oxide, **KBr** Potassium Bromide, **KCl** Potassium Chloride, **KI** Potassium Iodide, **KNO_3** Potassium Nitrate, **KPb_3** Potassium Lead Iodide, **MA** Methylammonium, **$(\text{MA})_2(\text{DMSO})_2\text{Pb}_3\text{I}_8$** non-perovskite solvate phase occurring during spin coating, **$\text{MAPb}(\text{I}_x, \text{Br}_{1-x})_3$** Methylammonium lead iodide/bromide (perovskite), **MAPbBr_3** Methylammonium lead bromide (perovskite), **MAPbI_3** Methylammonium lead iodide (perovskite), **N_2** Nitrogen Gas, **NaCl** Sodium Chloride, **Pb** Lead, **Sn** Tin, **SnO_2** Tin Oxide, **Spiro-OMeTAD** 2,2',7,7'-tetrakis-(N,N-di-p-methoxyphenylamine)-9,9'-spirobifluorene (hole transport layer), **Tol** Toluene.

1

Introduction

1.1 Photovoltaics and perovskites

1.1.1 PV basics

A solar cell (SC) generates electricity from sunlight by absorbing photons in the absorber material. The photons excite electrons in the semiconductor from the valence band to the conduction band where they ideally can move freely by diffusion and by influence of an electric field. The minimum difference in potential energy for an electron in the valence band and in the conduction band is known as the bandgap, which is material specific. The bandgap for silicon, used in standard SCs, is 1.12 eV while for perovskites it depends on the ionic composition of the material.

For a photon to excite an electron to the conduction band it needs an energy at least as high as the bandgap, hence photons with a too low frequency cannot be absorbed to generate current. When an electron has been excited, the newly gained electrical potential energy can partly be used in the external circuit (which is the purpose of a solar cell). The electron that has been excited leaves behind a vacancy in the valence band that will act as a pseudo-particle with positive charge, referred to as a hole.[2][3]

In order for a solar cell to be of any use, it needs to generate a net flow of electrons in one direction between the electrodes. Doping of the semiconductors with other elements or charge selective contacts are used to provide the electric field supporting charge separation between electrons and holes so that electrons are extracted at one contact and holes at the other. Standard silicon solar cells use doping of the silicon crystals for charge separation, while perovskite solar cells instead use charge carrier selective contacts where an electron transporting layer (ETL) and a hole transporting layer (HTL) are put between the perovskite absorber and the standard contacts.[2][3]

1.1.2 Perovskite basics

Research field

The increase in reported device efficiencies of solar cells based on metal halide perovskites has been very rapid compared to other types of solar cells, which explains

why they have become a hot topic for photovoltaic research.[4] The combination of high performance enabled by excellent optoelectronic properties of the perovskite materials, ease of material and device processing, and potentially low fabrication costs has led to continually increasing research efforts in perovskite solar cell (PSC) technology, accelerating the learning curve.[5]

What is a perovskite?

A perovskite is a material which possesses the same crystal structure as CaTiO_3 , namely the perovskite structure. A perovskite can be produced using many different elements but will always be a compound on the form ABX_3 . In halide perovskites used for photovoltaics, "A" is a monovalent cation and "B" is a divalent cation. By compositional engineering of perovskite semiconductors, a variety of materials and bandgaps can be achieved.

For photovoltaic purposes, the most common monovalent A-cations to use are formamidinium (FA), methylammonium (MA) and cesium (Cs). It is possible to use just one type of ion for each of the "A, B and X" ions in the perovskite lattice, or to use a mix of ions, e.g. letting the monovalent A-cation be a mixture of FA and MA. This means that there is an infinite number of different perovskite compositions that can be achieved, each with its own unique material properties. The divalent B cation is often lead (Pb), but lead-free perovskites are also possible by using tin (Sn) instead of lead. The X anion is often iodide, bromide, or a mix thereof. By bromide-iodide alloying, higher bandgap materials can be achieved.[4][6][7][8] In this project, changes in the bromide-iodide ratio is the only variation of the perovskite composition studied, while the cations are chosen to MA and Pb respectively in order to reduce complexity.

Challenges

While achieving specific perovskite compositions per se is not very challenging, the fact that each composition constitutes a new material that behaves differently from other compositions adds complexity to parameters that are challenging since research results may not be directly translatable between solar cells based on different perovskite compositions. Achieving stability similar to standard silicon solar cells is one of the main challenges for PSC development and this becomes further challenging when trying to achieve this for multiple material compositions that differ in their stability behaviors.

The stability issues of perovskites are both such concerning long-term aging effects (gradual decomposition), affected by humidity and temperature conditions etc. as well as short-term effects such as photo-induced instability that can be observed directly after fabrication and that is partly reversible.[9][10] There are also up-scaling challenges for perovskites in order to become industry friendly. These issues must be solved without too much compromise on manufacturing costs for perovskite SC technology to be able to compete with, or to improve, current market leading silicon technologies.[11]

1.2 Research Problem

The formation process of spin coated perovskite films is not yet fully understood. A more detailed understanding of how crystallization routes and final film morphology relate to perovskite precursor chemistry as well as to formation process parameters can help in optimizing high quality films for highly efficient perovskite solar cells.

1.3 Aim

The aim is to investigate how spin coating process parameters such as antisolvent treatment conditions (see section 2.3) and the chemistry of the underlying contact layer influence perovskite film formation, and how these parameters relate to final film quality and the resulting performance of solar cells. Further, the aim is to increase the understanding of how the film formation and resulting performance of the solar cells relate to the halide ratio in the perovskite precursor solution of mixed halide perovskites.

2

Theory

2.1 Bandgap tuning and wide-bandgap perovskites

2.1.1 Bandgap tunability and tandem application

The tunability of the bandgap of metal-halide perovskite semiconductors makes them a promising candidate to use in multi-junction solar cell technology. By altering the material composition of the perovskite crystals, the bandgap can be increased or decreased to fit the application whether this is a subcell for a tandem solar cell or a semi-transparent solar panel in the customer's favorite color. By gradually changing the ionic composition of the perovskite, the bandgap can also be gradually tuned, to achieve a perfect match for the desired application. In the world of perovskites, a "low-bandgap" semiconductor could have an absorption onset around 1.2 eV whereas a wide-bandgap could have an absorption onset more than twice as high.[4]

Since even the low-bandgap perovskites have higher bandgaps than silicon, for a silicon/perovskite tandem cell, a perovskite with a higher bandgap that can fit as a top-cell for a silicon bottom-cell is desired. For other applications however, a low-bandgap perovskite could be used alone in a single-junction solar cell or as a bottom-cell in a perovskite/perovskite double-junction device. For this reason, the whole spectrum of bandgaps is of interest for the photovoltaic research community. Using metal-halide perovskites for either one or both subcells in a tandem device has been identified as a promising approach to achieve scalable, low-cost tandem solar cells.[4] Though Photon conversion efficiencies (PCEs) of perovskite/silicon tandems exceeding 29% have already been demonstrated [12], perovskites with a bandgap of about 1.75 eV that should optimally be used for high-efficiency perovskite/silicon tandems are not easily achievable for practical use. Mixed bromide-iodide compounds with bandgaps higher than 1.7 eV tend to exhibit photo-induced phase segregation where regions with lower bandgaps are formed within the material. This has the effect that the maximum open circuit voltage achievable in devices is limited by the lower bandgap domains. This problem can be addressed by compositional engineering but is very apparent for the MAPb-based perovskites which are studied in this project.[4]

2.1.2 How to tune a bandgap

The bandgap of the perovskite correlates to the dimensions of the crystal, where a smaller lattice parameter gives a higher bandgap. A smaller crystal lattice in a perovskite semiconductor can be obtained by the utilization of halide anions with a smaller effective radius. This means that a bromide-based perovskite crystal has a higher bandgap than an iodide-based. By varying the halide composition, the bandgap can be tuned. Bandgap tuning of organic metal halide perovskites for solar cells obtained by varying the halide composition was first reported in 2013 by Noh et al. [6] who achieved this with the $\text{MAPb}(\text{I}_x, \text{Br}_{1-x})_3$ series, which is exactly the perovskite series studied in this project. The principle of bandgap tuning of perovskites by halide substitution is however not exclusive to MAPb-based perovskites but possible for all halide perovskites.[4]

From previous experiments on the $\text{MAPb}(\text{I}_x, \text{Br}_{1-x})_3$ series, it has been shown that compounds with a bromide ratio higher than 15% will at room temperature have a cubic crystal structure while those with a lower bromide content have a tetragonal crystal structure that is similar to that of MAPbI_3 . According to Unger et al. [4], there seems to be a clear trend for the negative covariation of lattice parameter and absorption onset for this perovskite series, based on several subsequent experiments from different laboratories, confirming the results from the first reported experiments by Noh et al.[6]. The trend is especially apparent for compounds with absorption onsets ranging from 1.6 to 1.8 eV, while the results differ more between data sets for absorption onsets exceeding this range. A possible explanation for the discrepancy shown for the extra high bandgap compounds is that these also show a higher ionic inhomogeneity [7] [13]. This is however not the case for pure bromide, which lacks the ionic inhomogeneity of the mixed halide crystals.[4]

2.1.3 Challenges for wide-bandgap PSCs

Hysteresis

Now that perovskite solar cells have reached efficiencies comparable to that of the market leading solar cell technologies, the next important step is to reach high operational stability. Among the most common device architectures for PSCs are thin-film devices with the perovskite layer processed on top of the n-type selective contact. These are referred to as regular or n-i-p devices.[1] A problem with n-i-p devices is that they generally exhibit considerable discrepancies between current-voltage measurements conducted in the forward scan direction compared to the reverse scan direction, that is from low voltage to high versus from high voltage to low.[14] This discrepancy between forward and reverse measurement is referred to as hysteresis and can be quantified by a hysteresis index (HI).[1] There are several different ways to define the hysteresis index, for the measurements in this project it will be defined according to equation 2.1:

$$HI = (PCE_{\text{rev}} - PCE_{\text{for}})/PCE_{\text{for}} \quad (2.1)$$

For an ideally behaving solar cell, there should be no difference in the current-voltage curve depending on scan direction and hence a HI of 0.

The mechanisms causing the hysteresis have been proposed to be a combination of charge carrier recombination, unbalanced charge transport, capacitive effects, and ion migration at the interface of the transport layer and the perovskite layer. [14] When it comes to the chemistry of the material, it has been suggested that ionic defects at the perovskite/metal-oxide interfaces and the accumulation and migration of ionic defects is the underlying cause of hysteresis.[15][16] Defects at the interface between perovskite and charge transport layer cause non-radiative recombination as well as making the quasi-Fermi level splitting disordered. This has the effect of a reduction in charge carrier concentration as well as decreasing the open circuit voltage (V_{OC}). This means that the mechanisms behind the hysteresis should have a negative impact on the performance of the solar cell device. However, the harm from ionic defect migration in the perovskite does not end with these direct effects on device performance, it has also been shown to be detrimental to device stability.[1] This means that current-voltage hysteresis is also an indicator of an unstable device.

Hoke effect

For higher bandgap mixed halide perovskites, a well observed but less well explained photo-induced phase-segregation hinders the achievement of the desired high open circuit voltage devices. The phenomenon has been referred to as the Hoke effect as Hoke et al.[7] used this explanation when observing photo-induced low-energy emission peaks in these materials from photoluminescence measurements. The phenomenon was also observed to partially reverse when the perovskite samples are left in the dark, which means there is a phase segregation in the material under illumination and a phase (re)homogenization when no longer exposed to light. The results from Hoke et al. were exciting news for those researchers who had already assumed that photo-induced halide migration should be a contributor to the current-voltage hysteresis observed in these materials, as these results constituted the first direct evidence for this.[4]

The Hoke effect more specifically means that under illumination, the halides segregate to form iodide rich and bromide rich regions. As the bandgap of the perovskite correlates with the concentration of iodide vs. bromide, the iodide rich regions create low-bandgap environments. This means that the excitons formed by excitation in a high energy, bromide rich region of the material can diffuse into the low energy, iodide rich phase which then acts as traps that limit the voltage that can be extracted from the solar cell device.

The onset of the Hoke effect is dependent on the material composition of the perovskite. Photoluminescence data shows that the $\text{MAPb}(\text{I}_x, \text{Br}_{1-x})_3$ series exhibits a Hoke effect, which means they emit light from a lower energy phase, for bandgaps above approximately 1.7 eV, while for example the threshold for the $\text{CsPb}(\text{I}_x, \text{Br}_{1-x})_3$ series seems to be around 1.9 eV. It is not fully understood what determines the threshold for the Hoke effect for a specific compound or the composition or energy level of the lowest emitting energy phase.

The high bandgap that seems achievable for some compounds without a clear onset of the Hoke effect might be an indication that alloys with higher crystallinity and ionic homogeneity can stabilize the phase homogeneity. Photoluminescence (PL) data show that the energy level of the PL emission peak from the iodide rich phase seems to be dependent on the cation of the compound. When the material is in the dark, a more homogenous ionic distribution will be thermodynamically favorable. However, When the material is illuminated the thermodynamics of the material is different and seems to favor a more heterogenous distribution. Some have argued it could be that the de-mixed states minimize the Helmholtz free energy in the case of illumination.[4]

Comparing the threshold for the Hoke effect as well as the energy level of the low energy phase to the bandgap energy levels where a phase shift normally would occur for the compound might give a clue to what happens in the material. For the MAPb(I_x, Br_{1-x})₃ series, these energy levels are about 1.68 eV, which corresponds to a bandgap for a composition with a lattice parameter of 6.22 Å, which is approximately the size of the crystal lattice for the ionic composition where the shift from tetragonal to cubic phase at room temperature is observed[6].

It is not yet entirely clear whether the Hoke effect is a process acting on already present inhomogeneities, or if the effect would be observed even if a perfectly homogenous crystal lattice was achieved. It is also not clear if low energy trap states are intrinsic to all compositions exceeding a certain bromide content or if they are created upon illumination. However, pre-existing inhomogeneities seem to be an important factor favoring low energy phases within the material and it has been found that the Hoke effect is suppressed in highly crystalline materials.

This suggests that the Hoke effect might be possible to avoid in high-bandgap alloys if very high phase homogeneity could be achieved. Halide inhomogeneities and low energy trap states are however likely to form in lead halide perovskites since the activation and formation energies of halide vacancies are relatively low. So even if a perfectly homogenous mixed halide perovskite is achieved, it is likely that inhomogeneities will still form spontaneously under operating conditions for a solar cell. The realization of Hoke-free, high-bandgap solar cells based on lead halide alloys might therefore not be realistic.[4]

2.2 Film formation process of mixed halide perovskites

Rehermann et al. [17] made a previous study on the film formation process of the MAPb(I_x, Br_{1-x})₃ perovskite series during spin coating and annealing with the same in-situ spectroscopy setup used to study film formation in this project. In their study, the same perovskite precursor mixes were used as in this project, but the spin coating was performed without the use of antisolvents. Rehermann et al.[17] found that there are two competing crystallization pathways that occur to different degrees during spin coating depending on the halide mix.

Pure bromide will crystallize directly into a perovskite phase during spin coating, while a pure iodide first forms an intermediate solvate phase, $(\text{MA})_2(\text{DMSO})_2\text{Pb}_3\text{I}_8$, after which it will change into a perovskite phase upon temperature annealing. These different pathways can partly be explained with iodide interacting more strongly with DMSO and further not coordinating as strongly to lead compared to bromide. For the 70% iodide mix, the pathway will look similar to the pure iodide, with an intermediate solvate phase forming that changes into the perovskite phase upon temperature annealing, with the difference that the incorporation of some bromide causes a delay in crystallization onset compared to for the pure iodide.

For the mixed halide solutions with 30% and 60% iodide, both film formation pathways will occur during spin coating, which means that a bromide enriched perovskite phase starts to form while some of the solution forms an iodide rich solvate phase, hence giving a heterogeneous mix of phases. The halide ratio of the bromide-enriched perovskite phase depends on the halide mix of the precursor solution, where a higher bromide content in the precursor solution gives a higher bromide ratio in the perovskite phase forming. The halide ratio also influences the crystallization onset of the perovskite where a higher iodide content gives a later onset for all the solutions forming a perovskite phase during spin coating.

During annealing, the solvate phase decomposes into an iodide rich perovskite phase, and ion exchange between the iodide rich perovskite phase and the bromide rich phase will occur. This results in more compositional homogeneity than directly after spin coating, but some ionic heterogeneity still remain after annealing. This co-crystallization of two different phases during spin coating can explain the ionic heterogeneity with iodide- and bromide enriched domains found in mixed iodide-bromide perovskite films. Ionic inhomogeneity pre-existing in the perovskite film from the film formation can contribute to the Hoke effect found in high-bandgap PSCs.

2.3 The role of antisolvent in film formation

Several methods have been reported for fabrication of high-efficiency PSCs, including spin coating, thermal evaporation, chemical vapor deposition, and spray coating. Spin coating of the perovskite precursor solution followed by antisolvent (AS) treatment to form the perovskite layer is a common method to fabricate highly efficient mixed halide PSCs, and is also the fabrication method used in this project.[18] AS treatment has been used for several of the reported world record efficiency devices.[19]

The working mechanism of antisolvents is speeding up heterogeneous nucleation by creating instantaneous local supersaturation on the substrate. The AS treatment process involves complicated interactions between the substances on the substrate that take place simultaneously and that depend on the physiochemical properties of the solvents in the precursor solution.[19]

So far, the most popular antisolvents used for perovskite film formation are toluene, chlorobenzene and diethyl ether. While these three solvents all have been shown

to perform well in the formation of different perovskite films, their physicochemical properties differ dramatically. Important to note is that they have not been evaluated for the same type of perovskite, which makes it difficult to fairly and properly compare them.[19] In this project toluene and ethyl acetate are the antisolvents used, and which one of these that is chosen in the specific case depend on the Br/I ratio of the perovskite precursor solution.

When comparing several antisolvents with spin coating of perovskites without AS, Paek et al.[19] found that antisolvents have a substantial effect on the crystal growth kinetics and the film morphology on a micrometer scale. The morphology of the perovskite film is one of the most important parameters that determine the final performance of PSC devices. The use of a suitable AS would give pinhole free homogeneous films while the number of holes in films formed without AS treatment were significantly more. They found that key parameters of the AS are boiling point, miscibility with the perovskite precursor solution, and the dielectric constant, where antisolvents with a higher boiling point and good miscibility with the precursor solvents (DMF/DMSO) will give PSCs with higher efficiency and higher reproducibility. They also found that the use of AS treatment in general lead to higher V_{OC} and that the solar cells with AS treatment, regardless of which one, had superior PCE compared to those made without AS treatment.

2.4 Interface modifiers

Several approaches have been investigated to resolve the issues linked to hysteresis, both efforts to reduce defects in the perovskite using additives, as well as attempts to modify the perovskite/metal-oxide interface.[15][16] Alkali salts as additives to the perovskite precursor solution have been shown to increase device performance and decrease hysteresis.[1] For this project, only the second approach with modification of the interface has been tried.

A few studies, including a study by Dagar et al. from the lab where the devices for the project have been fabricated, have used alkali salts as interface modifiers (IMs) by directly introducing them at the interface. [1] In the Dagar et al. study, they used the same experimental methods to introduce the IMs as we used in this project, as well as the same device architecture (ITO/SnO₂/IM/perovskite/Spiro/Au), though the perovskite compositions differed. The alkali salts were spin coated from aqueous solution (2.5 mg mL⁻¹) on the SnO₂ layer, prior to the spin coating of the perovskite layer.

The study found that all potassium salts tried (KI, KCl, and KNO₃) improved device performance, reduced hysteresis and increased the stability of steady-state performance. The salt leading to the highest PCE was KNO₃, which is therefore the first salt tried as IM in this project. The study also found that there was a correlation between the solubility of the potassium salt in the perovskite precursor solution and the benefit it had on device performance.

In the study, samples with NaCl as IM showed some increase in average PCE and reduction in HI compared to the control samples. Comparing the sodium-based

salts tested in this study, chloride as anion seems to be more beneficial than iodide, though sodium does not seem to make a substantial difference for device performance.

The potassium based salts tested in the study showed an improvement in average PCE as well as reduced HI compared to untreated samples, indicating that potassium as cation is beneficial for device performance. The average increase of PCE for devices with KCl as IM was 11% and for KNO_3 , which showed the best performance in the study, the average increase of PCE was 15%. The spread in short circuit density (J_{SC}) was slightly larger for devices with potassium salts compared to devices without or with other IMs. For both KCl and KNO_3 , the average V_{OC} , fill factor (FF), and PCE increased. KI as IM did however not show an improvement in PCE, but instead a slight decrease. The authors assume that the increased V_{OC} for KNO_3 devices is due to a reduction of charge carrier recombination at the interface. There was a strong reduction of HI for all K-based salts, which was attributed to improvements in charge carrier extraction efficiency at the n-type selective contact.

Other studies have added K^+ to the perovskite precursor solution and found an improvement in device performance and stability as well as a reduction in hysteresis. [20][21] However it was also found that when added to the perovskite precursor solution, the potassium would reside at interfaces or form secondary phases of KI, KBr or non-perovskite KPbI_3 rather than being incorporated to the perovskite crystal.[20] For that reason, it would make sense trying to put it directly at the interface.

Dagar et al. conclude from their results that KCl and KNO_3 as IMs seem to effectively suppress hysteresis due to ion redistribution. The phenomena related to the dynamic responses in perovskites, (internal charge carrier distribution, charge carrier trapping/de-trapping at interfacial defects, and ion migration), can cause dynamic capacitive effects that probably occur at different time scales. Surface photovoltage (SPV) measurements in the Dagar et al. study indicate that there is a large reduction in hole trapping at the SnO_2 /perovskite interface for samples with KNO_3 as IM compared to untreated samples, which is likely to be a reason for the improved device performance. Their findings indicate that potassium salts as IMs have a highly beneficial effect regarding compensation of interfacial charge-up and that they can improve interfacial charge carrier extraction. Exactly what mechanisms that lead to the improvements is however so far unknown. The increase in V_{OC} for KNO_3 modified devices is likely due to passivation of interfacial defects.[1]

3

Methods

3.1 Project outline

In order to help the reader to get a grasp of the project as a whole and of the motivation behind decisions regarding methods and experiments, here is a short summary of the project outline regarding the experimental parts in chronological order.

3.1.1 Learning and preparing characterization setups

The first practical part of the project was learning how to perform External Quantum Efficiency (EQE)- as well as current density-voltage (JV)-measurements with the setups at Lund University (LU) on standard PSCs made at Helmholtz-Zentrum Berlin (HZB). This was both for me to gain practical knowledge about the characterization methods as well as to prepare the setups in Lund to perform measurements on PSC-samples from HZB, as there was a plan to use these setups to measure HZB-samples both from this project as well as in the general HZB and LU collaboration projects. The solar simulator for the JV-measurements in Lund was completely new so part of this preparation was setting it up for use in general.

3.1.2 Perovskite film formation

At HZB the first part of the experiments was studying the perovskite film formation during spin coating with AS treatment, where various perovskite films were fabricated and characterized. The aim was to study the formation process and final film quality of the same type of perovskites ($\text{MAPb}(\text{I}_x, \text{Br}_{1-x})_3$) that subsequently would be used to fabricate solar cells. We made perovskite films with five different halide ratios in the precursor solution, including pure iodide, pure bromide, as well as three mixed halide films with different I/Br ratios.

Using in-situ UV-vis spectroscopy we studied how AS treatment and the type and timing of AS affected the crystallization of the perovskite film for the different halide ratios. The resulting film properties were also investigated using scanning electron microscopy (SEM) and (ex-situ) UV-vis. We first made one batch with perovskite films on glass substrates, which we measured both in-situ and ex-situ and then one additional batch where SnO_2 first had been deposited on the substrate (in order to

deposit the perovskite on the same material as we do on device level), which we only characterized ex-situ using SEM. From the results of the film formation experiments the type and timing of antisolvents that were tried when fabricating the solar cells were chosen.

3.1.3 Fabrication of solar cells

During the project we fabricated and characterized four batches of PSCs. For the first two, AS timing for the perovskite deposition was varied similar to in the previous film formation experiments, based on the results from these. For the third and fourth batch we then chose fixed AS timings that seemed reasonable based on the previous results. In the third and fourth batches, we additionally tried to further improve the solar cells by adding alkali salts as an interface modifier (IM) prior to the deposition of the perovskite, as this has previously been shown to be beneficial for the performance of some standard recipe PSCs at HZB [1]. JV-measurements were conducted on all batches and additionally some batches were characterized using Maximum Power Point (MPP) tracking, EQE, SEM (cross-sectional with side-view of the sample), and X-ray diffraction (XRD). Due to limited time and quality of resulting data, all measurements are not presented in the report.

3.1.4 Characterization of solar cells at Lund University

An attempt was made to transport the last two batches of solar cells to Lund, to characterize them with the setups there. Unfortunately, the software for the JV-setup at LU was still a work in progress as the samples arrived in Lund, with the consequence that the samples were measured more than a month after they had been fabricated. JV- as well as PL-measurements were carried out in Lund. We also tried to perform electroluminescence measurements but failed since the gold contacts on the samples were too easily torn off by the conductive tape that we used to connect them to the voltage source. Since the solar cells did not generate any photocurrent during the JV-measurements in Lund, the results of these measurements are not included in the report.

3.2 Fabrication methods

The perovskites used for all samples fabricated and studied in this project is the $\text{MAPb}(\text{I}_x, \text{Br}_{1-x})_3$ series with varying halide compositions. A total of four batches of PSCs were fabricated as well as two batches of perovskite films on substrates that were not further processed into solar cell devices but used to study film formation. These two batches of perovskite films are referred to as OB1-2 (Optical Batch 1-2) and the solar cell batches are referred to as SCB1-4 (Solar Cell Batch 1-4), with numbering in the order of date of fabrication. Not all batches in the project have been characterized with the same methods, but the samples themselves differ only slightly between batches, details about the differences are found in the following sections describing fabrication methods. Table S1-S6 with detailed information on all fabricated samples (OB1-2 and SCB1-4) can be found in the Supporting Information (SI).

3.2.1 Fabrication of perovskite films

The batches with perovskite films that were made to study film formation and morphology were fabricated similarly to the solar cell batches regarding the perovskite deposition. The process steps to make the optical batches are described in the following section. For OB1, the perovskite layer is deposited directly on a glass substrate. For OB2, the contact and charge transport layer that precedes the perovskite layer in the solar cell batches, are also included, meaning a pre-coated layer of ITO followed by a layer of SnO₂. The iodide to bromide ratios used in the perovskite precursor solutions for both of the optical batches are $X_{sol} = 0, 0.3, 0.6, 0.7$ and 1.

a) Preparing glass substrates

1) Numbering substrates

The substrates were numbered on the glass side with a diamond scribe pen, which is either of the sides for the plain glass substrates used for OB1 and the side without ITO for OB2. For OB2, substrates pre-coated with fully covering ITO were used.

2) Cleaning substrates

The numbered substrates were put in a glass staining trough.

- i) Mucasol 2% was poured into the sample holder to fully cover the substrates. The sample holder was put in an ultrasonic cleaner for 15 minutes.
- ii) The substrates were then cleaned with isopropanol and put in the ultrasonic cleaner for 15 minutes and subsequently dried with a N₂-gun.

b) Silver back mirror (OB1)

A silver layer was deposited using evaporation on the back side of the glass substrate for OB1 in order to have a mirror for the in-situ optical measurements. The silver mirror thickness was 80 nm. The substrates with silver back mirror were then put in the UV ozone cleaner prior to spin coating of the perovskite layer.

c) SnO₂ electron transport layer (OB2)

A layer of SnO₂ was deposited before the deposition of the perovskite. This step was included for OB2 only.

1) Spin coating

The substrates were spin coated with a solution of SnCl₂·2H₂O in ethanol with a concentration of 22.5 mg SnCl₂·2H₂O per ml ethanol. For each substrate 70 μl of SnCl₂-solution was spin coated twice, first one drop at 1500 rpm for 30 s, then a second drop at 2500 rpm for 30 s. This should give a total layer thickness of the SnO₂ of 20 nm. After spin coating, the substrates were put on a hot plate at 180°C for annealing. Oxygen from the air reacts with the tin on the substrate to form SnO₂.

2) The substrates are put in ozone plasma in the UV ozone cleaner for 25 minutes to improve film quality by cleaning and polarizing the surface.

d) Perovskite

While depositing the perovskite layer on OB1, in-situ UV-vis measurements were also performed in order to study the crystallization process, see chapter on characterization techniques for details. All steps for making the perovskite films were performed in N₂-gloveboxes.

1) Preparing solutions

i) Scaling solids

The solids used were PbI_2 , MAI, PbBr_2 and MABr. The solids were scaled and put in individual vials.

ii) Mixing with solvents

The solvent used for the perovskite solutions was a mixture of DMF and DMSO with the ratio 4:1 DMF:DMSO. The solvent was added to the vials with PbI_2 and PbBr_2 and the vials were then put in a shaking rack until all the solids were dissolved. The amount of solvent added was adapted to form solutions with a concentration of 1 M of PbI_2 and PbBr_2 respectively. The PbI_2 solution was added to the vial with MAI and the PbBr_2 solution was added to the vial with MABr so as to have solutions for MAPbI_3 and MAPbBr_3 respectively. The amount of solution added was also adapted to form solutions with a concentration of 1 M of MAPbI_3 and MAPbBr_3 respectively.

iii) Mixing perovskite solutions with different halide ratios

From the MAPbI_3 and MAPbBr_3 solutions, the solutions for the mixed halide perovskites, $\text{MAPb}(\text{I}_x, \text{Br}_{1-x})_3$, were obtained by mixing these solutions in different ratios.

2) Spin coating

The perovskite solutions were spin coated on the substrates at 4000 rpm for 60 s. The type of perovskite solution used for each sample can be seen in Table S1-S2 in SI:1. As AS either toluene or ethyl acetate was used with different drip timings. The type and timing of AS for each sample can also be found in the SI. The amount of AS per sample was 150 μl . While the perovskite solution was placed on the sample prior to starting the rotation program of the spin coater, the antisolvents were dripped during the spinning. After spin coating, the samples were put on a hot plate for annealing at 100°C for 30 min.

3.2.2 Device architecture

All SCs fabricated had a n-i-p structure and only small changes were made for the subsequent batches from the structure of the first batch. The first and second batch had the following layout from the front to the backside of the solar cell, which also corresponds to the order in which the layers were fabricated:

- Glass substrate with pre-coated and pre-structured (laser scribed) ITO
- SnO_2 as electron transport layer
- Perovskite $\text{MAPb}(\text{I}_x, \text{Br}_{1-x})_3$
- Spiro-OMeTAD as hole transport layer
- Gold as back contact

For SCB3-4 some solar cells additionally to the just mentioned layers had an IM alkali salt between the SnO_2 and the perovskite. The IMs used were KNO_3 , KCl , and NaCl respectively. See solar cell stack in Fig. 3.1. Every substrate used for solar cell fabrication contained six individual photovoltaic (PV) devices with an area of 0.16 cm^2 each, which was ensured by the structure of the laser-scribed ITO, see Fig.3.2. The halide ratios in SCB1-2 were $X_{sol} = 0, 0.3, 0.6, 0.7$ and 1, where X_{sol} is

the iodide ratio in the perovskite precursor solution. These were the same ratios as used for the optical batches. For SCB3-4, the 0.7 mix was changed to 0.8 in order to achieve a more even spread.



Figure 3.1: The solar cell stack, with the front side of the solar cell at the bottom in the figure. The alkali salt layer is only included for batches 3-4.

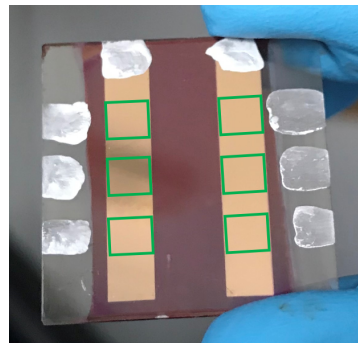


Figure 3.2: Sample viewed from backside with gold back contacts covering the solar cell active areas which are marked in green. Silver paste is added on contacts where they are connected to measuring tools.

3.2.3 Device fabrication

Some of the fabrication steps for the devices are the same as for the optical batches, in which case the reader is referred to the previous section about film fabrication for optical batches.

a) Preparation of ITO-coated glass substrates

1. Numbering substrates

The substrates were numbered on the glass side with a diamond scribe pen.

2. Cleaning of substrates

- i) Mucosal 2% was poured into the glass beaker containing the substrates, fully covering the substrates. With Mucosal the beaker was put in an ultrasonic cleaner for 15 minutes at 40°C.
- ii) Mucosal was replaced with distilled water and the beaker with substrates was put in the ultrasonic cleaner for 15 minutes.
- iii) Distilled water was replaced with acetone and the beaker was put in the ultrasonic cleaner for another 15 minutes.
- iv) Acetone was replaced with isopropanol and the beaker was put in the ultrasonic cleaner for 15 minutes.
- v) The substrates were dried with a nitrogen gun and put in a UV ozone cleaner for 15 minutes.

b) SnO₂ electron transport layer

This step was performed with the same procedures as for the optical samples, see the section on fabrication of perovskite films for details. For the solar cell samples a last third step was also included:

- 3) The SnO₂ film was removed from the substrates on the sides where the front contacts are according to Fig. 3.2. This is performed using a swab with ethanol.

c) Interface modifier (SCB3-4)

For some samples an IM was deposited on the SnO₂ before the deposition of the perovskite. For SCB3, half of the samples were spin coated with a layer of KNO₃ while the other half of the samples did not have any IM. The solution for spin coating was prepared from mixing KNO₃ with distilled water with a concentration of 2.5 mg KNO₃ per ml of water. The vial with the solution was put in a shaking rack at 25°C for the salt to completely dissolve. The samples were spin coated with 100 μl of the KNO₃ solution each. After spin coating the samples were put on a hot plate for annealing at 120°C. For SCB4, half of the samples were made with KCl as IM and the other half with NaCl, the same process was used for SCB4 as for SCB3.

d) Perovskite

The fabrication of the perovskite film was performed with the same procedures as for the optical samples, see the section on fabrication of perovskite films for details. The halide mixes used for the solar cells were $X_{sol} = 0, 0.3, 0.6, 0.7$ and 1 for SCB1-2 and $X_{sol} = 0, 0.3, 0.6, 0.8$ and 1 for SCB3-4. For SCB1-2 80 μl of perovskite precursor solution was used per sample and for SCB3-4 100 μl was used.

e) Spiro-OMeTAD hole transport layer

The Spiro solution was spin coated on top of the perovskite at 1800 rpm for 30 s. 80 μl of Spiro solution per sample was used.

f) Gold back contact

The gold contact was evaporated on the sample in a vacuum chamber at 10⁻⁶ mbar. A mask was used to make sure the gold is only deposited where the back contacts should be. A layer thickness of 80 nm was deposited.

3.3 Characterization techniques

3.3.1 In-situ UV-vis

In order to study the crystallization process of the perovskite layer during spin coating an in-situ spectroscopy setup was used. With this setup the UV-vis transmittance of the sample is tracked with sub-second resolution during the spin coating process. The in-situ measurements can give information about film formation kinetics, pathways and intermediate phases as well as the final film morphology. For this project the main focus was to use it to study the crystallization onset for different perovskite precursor solution mixes under varying AS treatment conditions.

A schematic of the setup can be seen in Fig. 3.4. The in-situ UV-vis setup consists of a white light halogen lamp (Thorlabs SLS201L/M) outside the glovebox as the light source which is coupled with neutral density filters on the inside of the glovebox to adjust light intensity. Optical fibers lead the light to the reflectance probe (Ocean Optics QR400-7-UV-BX) mounted just above the spin coater where the sample is prepared. The light leaves the tip of the reflectance probe through its center fiber, about 1 cm above the sample, and a silver mirror on the backside of the sample enables part of the non-absorbed light to reflect back and be collected via several small collection points around the center of the reflectance probe tip. The measure-

ment mode used is called transfectance since the signal consists of a combination of the transmitted and reflected light (see schematic in Fig. 3.3). Absorptance refers to the ratio of the light that is not collected, consisting of the light absorbed or scattered by the film. The collected light is led to a spectrometer (Ocean Optics Flame FLMS12200) outside the glovebox and the obtained data is processed by a connected computer.

Transflectance



Figure 3.3: Schematic of transfectance. Adapted from [22]

With this in-situ setup it is also possible to measure transfectance during annealing or to study photoluminescence of the sample, but within this project only UV-vis during spin coating was studied. From the spectrometer the transfectance of each wavelength over the measured time is obtained. The measurement ideally starts exactly when the perovskite precursor solution is dripped on the substrate, but since this must be done manually there is always a small difference between actual drip time and the onset of measurement which affects when crystallization seems to occur.

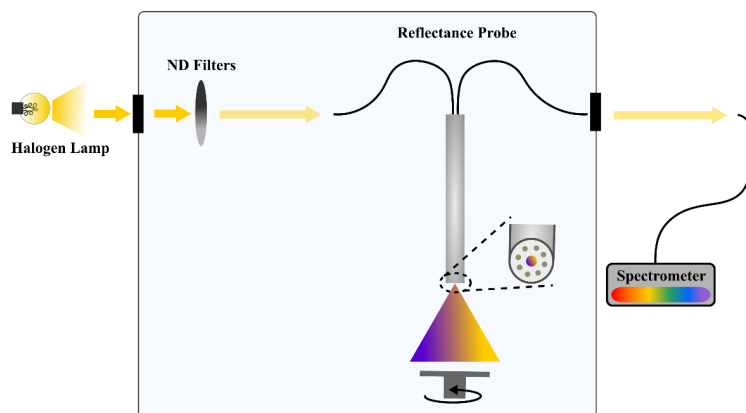


Figure 3.4: Schematic of in-situ UV-vis setup. Adapted from [22]

3.3.2 Scanning electron microscopy (SEM)

SEM uses electrons instead of photons, which allows for a higher resolution of the resulting images compared to an optical microscope because of the shorter wavelengths of electrons. The sample is put in a vacuum chamber where an electron beam is scanned over the surface. The electrons interact with the sample surface and as the electrons are collected, they can be used to create an image of the surface. The sample is being electrically connected to a sample holder (in our case with conducting copper tape) so that electric charge will not be accumulated during measurements. The sample holder is a metallic flat surface, allowing for different shapes and sizes of probes.

SEM has been used for two different types of measurements of samples in this project. First it has been used for the perovskite films in the optical batches with a top-down view on the perovskite surface. With this view the morphology of the perovskite film can be studied in terms of grain size, coverage etc. Estimations of film quality from these images helped to determine the fabrication parameters of the perovskite layer in the solar cells.

For the solar cells in SCB3, SEM was used to acquire side-view cross-sectional images of the solar cell samples. With cross-sectional images it is possible to see where the perovskite film is not in contact with the underlying layer, which can be seen as “holes” in the film at the interface. This is interesting since the holes limit the contact area where charge extraction can take place.

3.3.3 Current-Voltage analysis (JV)

Several characterization methods have been used within this project, but most emphasis both in terms of quantity of measurements as well as data analysis has been on current density-voltage (JV) measurements. In JV-measurements the solar cell is connected to a voltage source that scans over a preset range of voltage biases while simultaneously a solar simulator is used to shine light with a preset spectrum.

The resulting current from the solar cell is measured for each voltage step in the range and with the active area of the solar cell defined, the result is a current density per active area vs. voltage curve. With the software of the JV-setup immediately providing the plotted curve while the measurement is performed, and given it is known what the characteristic JV-curve of a solar cell looks like, it is possible to estimate how far from ideal the solar cell is behaving already while measuring. An example of a JV-scan for one of the solar cells fabricated in this project can be seen in Fig. 3.5.

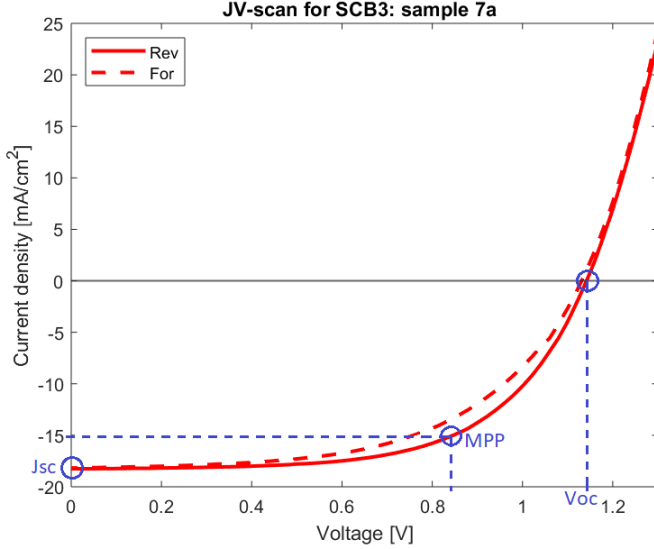


Figure 3.5: Example of a JV-scan for a solar cell with the forward scan as a dashed line. The Maximum Power Point (MPP) for the reverse scan is marked as well as the V_{OC} and J_{SC} .

Some performance parameters derived from the JV-scan are provided directly by the JV-setup software. Among these, J_{SC} , V_{OC} , PCE and FF are presented in the project. While the values of J_{SC} and V_{OC} can be seen directly from the scan plot, PCE is derived from the Maximum Power Point (MPP), which is the point on the curve where the resulting power (i.e. $J \cdot V$) is the highest. The FF is calculated as the product of the current density and voltage at the MPP divided by the product of the open circuit voltage and the short circuit current density, as seen in Eq. 3.1.

$$FF = \frac{J_{MPP} \cdot V_{MPP}}{J_{SC} \cdot V_{OC}} \quad (3.1)$$

These mentioned parameters are derived for each scan direction. When the values of the scan directions are not differentiated in the presented results, the value presented is always the mean value of the forward and reverse scan for a SC.

One way to spot and quantify non-ideal behavior for a solar cell is to evaluate the difference between the JV-curve that scans from low voltage to high voltage (the forward scan), and the curve when scanning in the other voltage direction (the reverse scan). Both scan directions are always measured and for three out of four batches of solar cells in this project, the reverse scan direction has been performed first, followed by the forward scan. The discrepancy between these curves is referred to as hysteresis and can be quantified with a hysteresis index (HI), see Eq. 2.1.

In order to perform a JV-measurement, not only the start and end values for the applied voltage need to be provided but also other inputs such as the size of each voltage step and the delay time after each voltage step prior to measuring the resulting current. Although for an ideal solar cell, only the start and end values should influence what the JV-curve looks like, given several non-ideal behaviors in PSCs, what these input variables are set to can give quite different results. The differences in these results when changing scan conditions can give clues to what mechanisms

are taking place in the cells and hence to the cause of non-ideal and unstable behavior of the solar cell.

It is known that several different phenomena cause hysteresis to different extents, and it is also known that the time-scale on which those phenomena occur differ. By changing the scan rate for the JV-measurements, it is possible to get a hint on what time scale the mechanism causing hysteresis act, and hence which phenomenon that might be. For example, hysteresis in a fast JV-scan performed on a much smaller time scale than a particular phenomenon potentially causing hysteresis can occur, must be caused by some other mechanism which takes place on a smaller time scale. In this project hysteresis is one of the performance parameters that has been studied, and in order to provide more information on this, most solar cells have been measured with several different scan rates. However, all results presented in the report are based on JV-scans with a delay time of 40 ms between each voltage step and the subsequent measuring of the current.

For all JV-measurements in this project the global standard spectrum, AM1.5G, has been used, which resembles normal conditions for a solar cell in use in clear weather. Dark-JV measurements were also conducted, meaning the measurements are performed in the same manner but without shining light on the solar cell, providing a JV-curve without photocurrent. Dark-JV cannot tell if the solar cell performs as a solar cell, i.e. generating photocurrent, but it shows the electrical behavior without light absorption. The dark-JV curve should look like a diode if it works normally, which is far from always the case when making non-standard PSCs.

In the project a total of three JV-setups have been used, two at the Helmholtz Zentrum in Berlin, Germany, where the solar cells were manufactured, and one setup at the physics department of Lund University, Sweden. All results from JV-measurements presented in the report are from measurements at the setups in Berlin.

3.3.4 Data analysis

All calculations for data analysis have been made using Excel or MATLAB, and all plots are created in MATLAB. The MATLAB code for the in-situ UV-vis plots presented was provided by my lab supervisor Carolin Rehermann. The reasoning behind the selection of solar cell data excluded from the presented results can be found in SI:4.

Analysis of cross-sectional SEM-images for the estimation of hole fraction of the film has been made with ImageJ. When estimating the hole fraction of the film using ImageJ, a tool for measuring distances was used to measure the length of each hole. The start and end point of each hole was estimated visually as automatic threshold based tools did not provide sufficient accuracy. Since the images only show the cross-section of each hole, the estimations of the hole fractions are based on one dimensional measurements of the holes.

4

Results and discussion

4.1 Antisolvent treatment in film formation

In the first study that was carried out within this project we focused on the film formation of the $\text{MAPb}(\text{I}_x, \text{Br}_{1-x})_3$ perovskite series and the role of AS treatment on film formation. The main part was studying the film formation in-situ with an optical tracking setup while carrying out the spin coating of the perovskite layer. The film formation without any AS was first studied, which shows the natural crystallization onset for the particular halide mix. Knowing when the crystallization occurs, AS drip times can be chosen, as the AS drop should be set before the self-crystallization. For each mix one or several drip times were tried and studied. Using the in-situ results together with SEM images of the resulting film surfaces, the AS treated samples can be compared to the non-treated samples as well as to other AS drip times. Additionally, samples were made with SnO_2 as the underlying surface to spin coat the perovskite onto as the perovskite is spin coated on a SnO_2 surface when making solar cell devices. Lastly, the effect of AS timing was tested on device level to see if and how it influences device performance.

4.1.1 Film formation

In this section the results of the optical in-situ film formation tracking results together with SEM images of resulting films are presented for each halide mix included. For all halide ratios, except for the 70% iodide mix, for which the in-situ experiment partly failed, six images are presented. The leftmost images are 2D-plots of the in-situ tracking, showing the time from when the spin coating of the perovskite precursor solution starts on the x-axis, and photon energy on the y-axis. The colorbar shows the proportion of photons that are absorbed or scattered by the film and thus not reflected back to the detector, referred to as absorptance. The initial color of dark blue indicates that all the photons pass through the wet film and are reflected back to the detector from the silver mirror at the backside of the sample. Shifts in color indicate increased absorption and/or scattering from the sample as the crystallization starts. The upper heat map shows a sample without AS treatment and the image below shows one of the AS treated samples. The upper middle image shows the absorptance spectra at $t = 60$ s, where the blue graph is the sample without AS treatment and the graphs with other colors are samples with AS treatment. The samples are represented by the same respective color in the plot below, showing the

absorbance evolution over time, averaged over a range of wavelengths. To the right the SEM images of the resulting film surfaces of the two samples represented to the left are shown. In SI:2, additional SEM images including more AS drip times as well as the samples spin coated on SnO_2 can be found.

MAPbBr₃

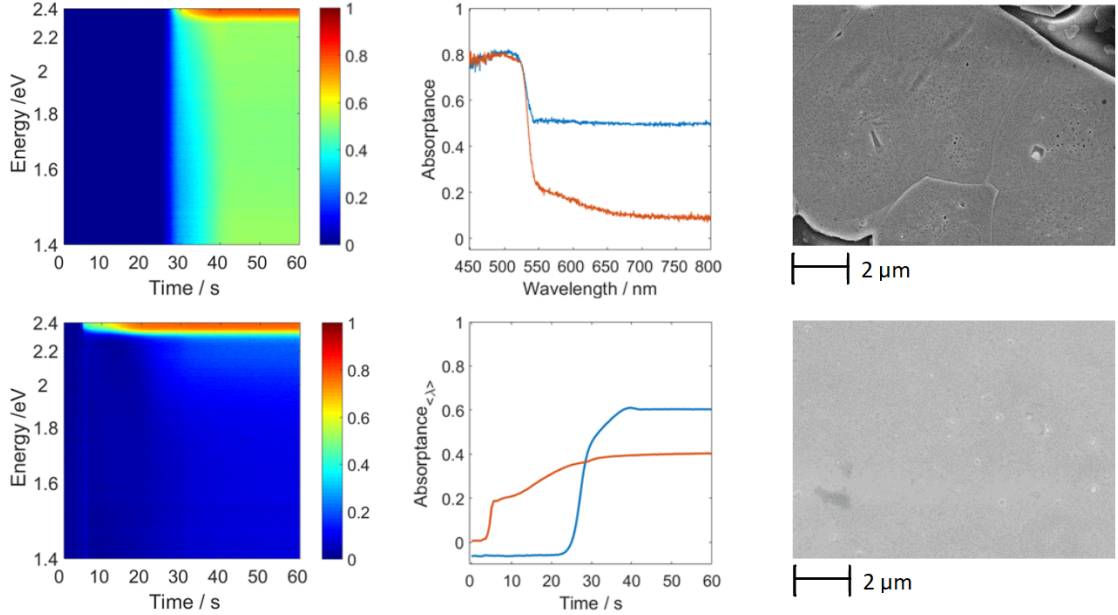


Figure 4.1: In-situ optical monitoring during film formation for the $X_{sol} = 0$ solution, and SEM images of resulting films. The images to the left show the formation process of a sample without AS (upper image) and with an AS drop at $t = 5$ s (below). The upper middle image shows the absorbance spectra at $t = 60$ s for the two cases, blue showing the sample without AS. The image underneath shows the development of the averaged absorbance over time. The SEM images to the right show the resulting film morphology of the sample without AS and the sample with AS (below).

In Fig. 4.1 the evolution of the optical signal during spin coating of a MAPbBr₃ sample can be seen. The upper left image shows a change in the optical features after about 25 s with an edge around 2.3 eV, but also a decrease in the optical signal for longer wavelengths. The edge at 2.3 eV can be attributed to the absorption onset of the MAPbBr₃ crystal which is a high bandgap perovskite, while the baseline shift indicates increased scattering from the sample. Since the self-crystallization of the sample occurs around 25 s after the onset of the spin coating, a suitable AS drip time should be before this. The lower heat map shows the film formation with an AS drop at 5 s after the spin coating is initiated. In this image, the baseline shift is very slight compared to the upper image. This difference can also clearly be seen in the absorbance at 60 s plot (the upper middle image) where the blue line shows much higher scattering for the longer wavelengths not absorbed by the perovskite. The difference in scattering between the samples indicates that the film surface of the sample with no AS is rougher compared to the AS treated sample. In most cases a smooth surface is preferable on device level and indicates a higher quality film.

The SEM images also confirm the results from the in-situ measurements, showing that the AS treated sample has a closed film with a smoother surface compared to the non-treated sample. These results indicate that using AS treatment improves film quality when forming a pure bromide perovskite. In Fig. S1 in SI:2, SEM images also show a sample with $t_{AS} = 15$ s next to the 5 s sample which also has a closed film but with some more surface defects visible compared to the 5 s sample. This indicates that early crystallization might be beneficial for the film quality. In the same image, films spin coated on a SnO_2 surface show closed and rather smooth films both in the case without AS and in the case with AS, but with a more spotty surface on the sample without AS treatment. From this it seems like the difference in film quality between AS treated films and non treated films might be smaller when spin coated on a SnO_2 surface as compared to when they are spin coated directly on glass substrates.

MAPb(I_{0.3},Br_{0.7})₃

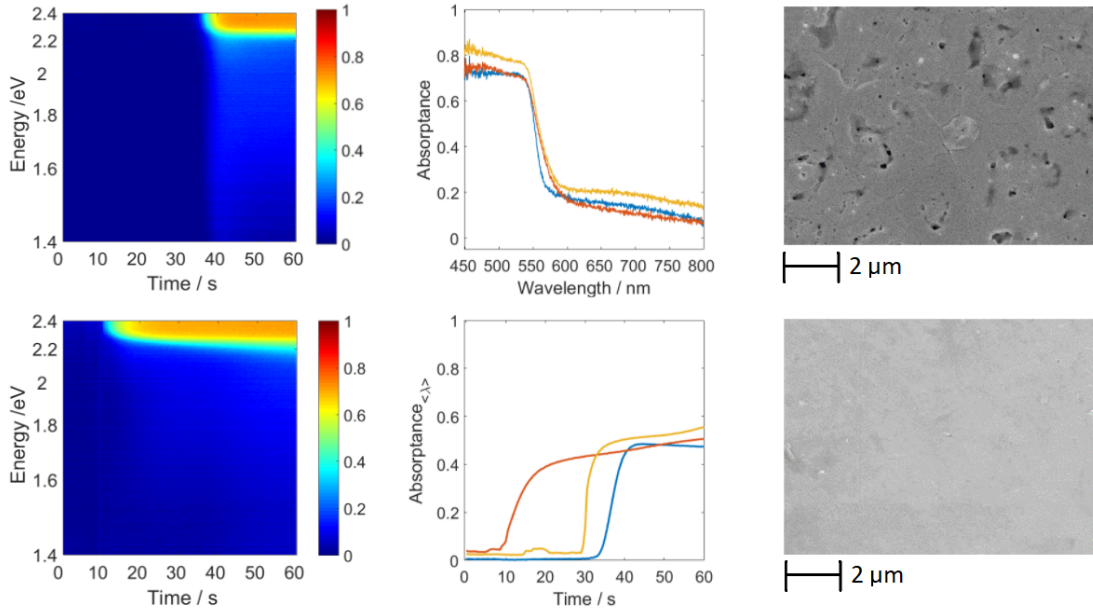


Figure 4.2: In-situ optical monitoring during film formation for the $X_{sol} = 0.3$ solution, and SEM images of resulting films. The images to the left show the formation process of a sample without AS (upper image) and with an AS drop at $t = 10$ s (below). The upper middle image shows the absorbance spectra at $t = 60$ s for the two cases and an additional AS timing, blue showing the sample without AS and orange and yellow showing the cases with AS timing of 10 and 30 s respectively. The image underneath shows the development of the averaged absorbance over time. The SEM images to the right show the resulting film morphology of the sample without AS and the sample with AS at $t = 10$ s (below).

With 30% iodide, the in-situ heat map shows a similar evolution for the AS treated sample as for the pure bromide sample. Also in this case there is a visible baseline shift at the crystallization onset for the sample without AS, indicating more scattering of the light and hence a rougher surface of the sample, but the shift is only slight and in the absorbance spectra at 60 s, there is no clear difference between the three cases of AS conditions tested. However, from the SEM images we can see that

the AS treated film is closed and quite smooth while the non-treated film is rough with big defects and possibly pinholes. Also in this case, it seems like AS treatment improves film quality.

For this mix it seems that an early AS drop at 10 s gives a somewhat slower nucleation process compared to an AS drop closer to the natural crystallization onset. Without AS treatment, the crystallization onset is at about 35 s, which means the range of suitable drip times is before 35 s. The SEM images seen in Fig. S2 show that both AS timings seem to produce closed and somewhat smooth films, the difference between the two is too small to say which timing would be preferable. For this halide mix, both the film with and without AS treatment fabricated on a SnO₂ surface are closed and somewhat smooth.

MAPb(I_{0.6},Br_{0.4})₃

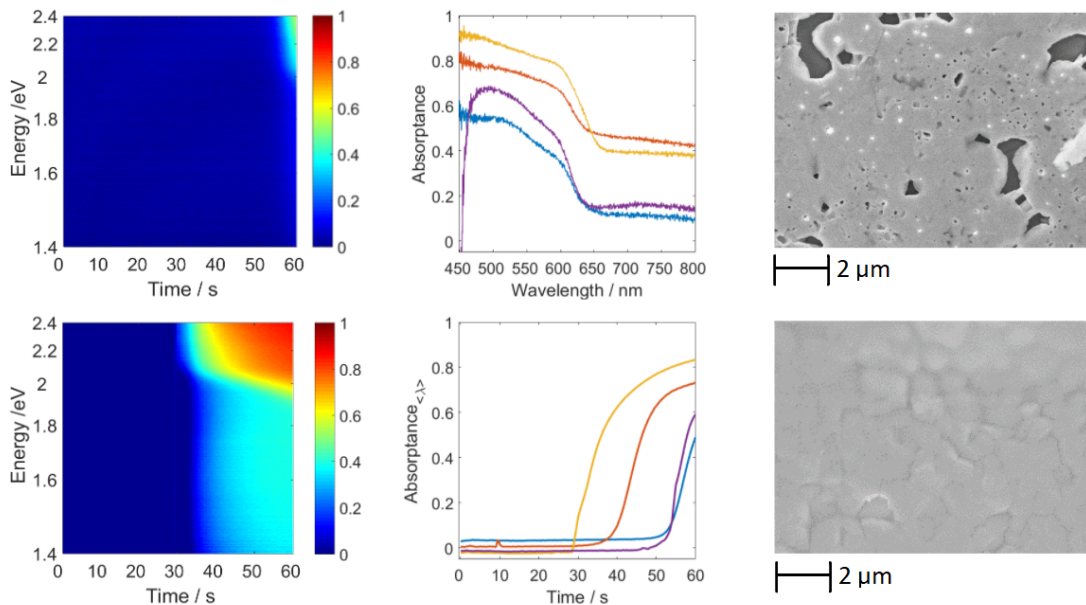


Figure 4.3: In-situ optical monitoring during film formation for the $X_{sol} = 0.6$ solution, and SEM images of resulting films. The images to the left show the formation process of a sample without AS (upper image) and with an AS drop at $t = 30$ s (below). The upper middle image shows the absorbance spectra at $t = 60$ s for the two cases and two additional AS timings, blue showing the sample without AS and orange, yellow and purple showing the cases with AS timing of 10, 30 and 55 s respectively. The image underneath shows the development of the averaged absorbance over time. The SEM images to the right show the resulting film morphology of the sample without AS and the sample with AS at $t = 30$ s (below).

The natural crystallization onset for the 60% iodide mix is after about 55 s, which means it is barely visible in the heat map using a time range of 60 s. It is, however, easily seen in the averaged absorbance plot. In the extended time heat map, see Fig. S6 in SI:3, it can be seen that there is a baseline shift in the no AS case which indicates a rough surface. This is confirmed by the SEM image showing a low quality film with several pinholes and defects. Also for this mix, the SEM image shows a smoother, higher quality film for the AS treated sample. Noteworthy in this case is

that an AS drop set as early as after 10 s did not initiate immediate crystallization, as seen in the averaged absorptance plot, but instead the crystallization occurs after about 40 s, which is even later than for the sample with an AS timing of 30 s. The small bump on the red graph in the averaged absorptance graph shows the timing of the AS drop. Still the AS drop at 10 s clearly initiates earlier crystallization compared to the no AS case. This result indicates that for ionic compositions with a late natural crystallization onset there is a limit to how early an AS drop can be set in order to immediately induce crystallization. Further experiments would be needed to confirm if this is the case.

The resulting films of the samples that were treated with AS after 10 s and 30 s respectively, as seen from the SEM images in Fig. S3, are both quite smooth without any major visible defects, showing a similar film quality for both AS timings, both clearly exceeding the film quality of the sample not treated with AS. It looks like both an early and a later AS drop improves film quality in a similar way, indicating that immediate initiation of crystallization from the AS probably is not necessary in order to improve film quality. When an AS drop is set at 55 s, around the natural crystallization time, the AS does not seem to impact the time of crystallization. However, it seems like it could produce a slightly more rapid process once initiated. There is unfortunately no SEM image for this AS timing to show the resulting film.

For the 60% iodide mix, the films on SnO₂ do not look as smooth as the ones spin coated on glass, both showing some larger surface defects. However, it looks like the sample with AS treatment has somewhat smaller defects compared to the no AS sample. In the case of this mix, it looks like the underlying surface that the perovskite layer is spin coated on might have a bigger influence on the resulting film quality, where the perovskite films spin coated on SnO₂ give a worse film quality than when spin coated on glass. In this case it would be very interesting with in-situ results for the samples spin coated on SnO₂ to see if the crystallization of the film with AS at 10 s is delayed also when spin coated on another surface.

MAPb(I_{0.7},Br_{0.3})₃

For the $X_{sol} = 0.7$ mix, the in-situ measurements for a sample without AS treatment failed and thus the results are not included in the report, see Fig. S7 in SI:3 for some of the plots. A couple of things can be mentioned about the results of the AS treated samples. We see from the heat maps of the sample with an AS drop at 10 and 30 s respectively, that there is a baseline shift, indicating the formation of a crystalline phase. However, there is no optical feature within the range of wavelengths measured, which would be the case for a perovskite crystal. This means that the phase is not a MAPb(I_{0.7},Br_{0.3})₃ perovskite phase. Likely, this is an intermediate non-perovskite solvate phase, possibly the (MA)₂(DMSO)₂Pb₃I₈ solvate phase earlier reported by Rehermann et al.[17], but this would need to be confirmed by examining the crystal structure using for example XRD.

What we also can see in Fig. S7 is that when toluene is used as AS at 30 s it does not seem to induce any crystallization. When it comes to the resulting films, see Fig. S4, toluene treatment after 30 s seems to lead to many big holes in the

film, which is also an indicator of toluene not being a suitable AS choice for high iodide mixes. The sample without AS treatment (Fig. S7) also has many holes and defects. The films with EtAc as AS, at 10 s and 55 s respectively, are both closed but not very smooth. On the SnO₂ samples, both the AS treated film and the non treated film look smooth and do not have any visible defects. For the 60% mix the films were clearly of lower quality on a SnO₂ than on glass, while for the 70% mix we see the opposite. Further experiments are needed to verify that the SnO₂ layer is a better underlying surface for some ionic compositions of the perovskite precursor than it is for others.

MAPbI₃

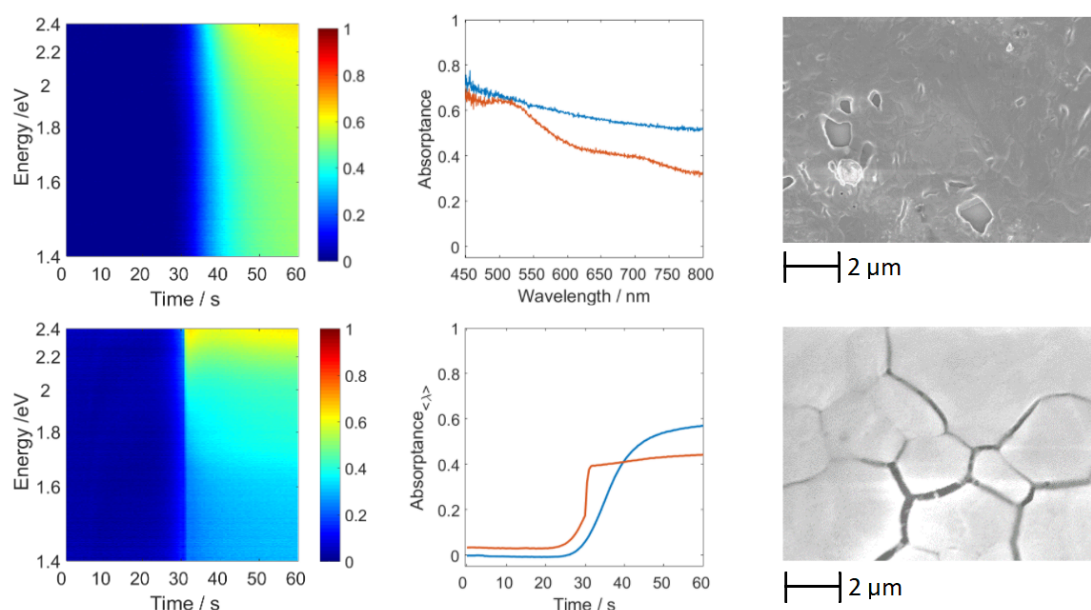


Figure 4.4: In-situ optical monitoring during film formation for the $X_{sol} = 1$ solution, and SEM images of resulting films. The images to the left show the formation process of a sample without AS (upper image) and with an AS drop at $t = 30$ s (below). The upper middle image shows the absorbance spectra at $t = 60$ s for the two cases, blue showing the sample without AS and orange showing the sample with AS. The image underneath shows the development of the averaged absorbance over time. The SEM images to the right show the resulting film morphology of the sample without AS and the sample with AS (below).

For 100% iodide, an AS drop set at around the natural crystallization onset at 30 s does not affect the onset timing but seem to initiate more rapid crystallization, similar to the 55 s drop for the 60% mix. In the heat map it is clear that there is a more gradual change in the no AS case while the change is very abrupt in the AS case. It should be noted however, that the baseline shift is so sharp that this could instead be due to measurement errors. What we see for the 100% iodide mix both in the heat maps and in the absorbance plot at 60 s is that there is no optical feature within the investigated spectra, showing that it is not the MAPbI₃ perovskite being formed. Again, we speculate that this is a solvate phase, based on the results of the Rehermann et al. study [17]. The results in this project show that the formation route with a solvate phase forming during spin coating is probably

the preferred formation route also when using AS treatment. Interestingly, it looks like the AS drop is beneficial to film quality also in the case where it only speeds up the crystallization of the intermediate phase which means high film quality of the intermediate phase film probably translates into a higher quality of the subsequently formed perovskite film.

It should be noted that SEM images with 10kx magnification level are lacking for the AS treated sample on glass for this mix, see Fig. S5, which means it can be that there are defects also for this film that are not captured at the greater magnification level, as is the case for the no AS sample. From the 10kx magnification level image of the no AS sample, it is clear that the film has several larger holes. The larger cracks between crystals in the image of the AS treated samples is likely due to the SEM characterization and not related to the innate film.

From the SnO₂ samples it is even more evident that the untreated sample has many large holes in the film and also an overall uneven surface. The AS treated sample looks similar, also with several holes and an uneven surface, however the holes of the 30 s AS timing sample are significantly smaller than the holes of the no AS film. From the SEM images it looks like AS treatment improves the film quality for the pure iodide perovskite both when spin coated on glass and on SnO₂. From the SnO₂ sample we can see that the film quality of the AS treated sample is still quite low, it may be that earlier AS timings would produce closed, hole free films.

4.1.2 Antisolvent drip timing on device performance

The effect of AS drip timing on solar cell device performance was investigated. The resulting performance in terms of J_{SC} and V_{OC} can be seen in Fig. 4.5. The resulting J_{SC} and V_{OC} plotted for each SC is the mean value of the forward and reverse JV-scan. Many solar cells either failed completely to generate photocurrent or had a JV-curve deviating too much from the characteristic solar cell behavior to be considered as reliable data and were hence discarded from the presented data set, only those remaining are seen in Fig. 4.5. SI:4 includes an explanation on how the solar cells were categorized to have acceptable JV-behavior and be included, or too deviating and be discarded from the presented data. Further I will simply refer to the solar cells included as functioning devices.

The large proportion of non-functioning devices unfortunately resulted in too little remaining data to draw reliable conclusions regarding which timing of the AS drop that produces the best perovskite layers at device level for each of the halide mixes.

In the plots the blue, red, and green dots represent devices from the first, second, and third batch of SCs respectively. It can clearly be observed that in some cases the average difference in the results between the batches for the same AS drip time exceeds the difference in results between different AS timings. This makes it difficult to attribute any observed difference in results to the drip times. Additionally, results within the same batch and timing are not independent as there are six devices on one single fabricated sample, meaning that some of the data points in

the plots represent devices from the same sample and what looks like a statistical difference between AS timings could be random differences between different samples, unrelated to AS timing.

Being aware of the shortcomings of the quality of the results presented, a few observations can be made which potentially can give some hints to what can be studied further. Overall it seems like the AS timing for the cases observed only slightly influences the performance. The optimal AS drip timing seems to depend on the precursor solution composition. Within the scope of this project, insufficient experimental data was obtained to enable validation of a clear trend. Here it should be noted that other important differences in SC performance not captured in this type of experiment can exist, such as long term stability. For low quality devices such as those made in this project, these differences are small as compared to random differences in quality between samples. However, it can still be an important factor to further investigate, as any slight improvement in performance is valuable in the development of high performance devices.

There are only very few pure bromide devices that can be compared and the differences in performance between drip times are also mainly between batches, meaning it is unclear if the observed differences are actually a result of drip timing. We can see that the current density seems to be slightly higher using an earlier AS drop. Also considering the SEM images of pure bromide samples in the SI, Fig. S1, where the film is smoother for the 5 s AS timing, it looks like the 5 s timing gives somewhat better results than 15 s drip time. For the $X_{sol} = 0.3$ mix, most of the devices with $t_{AS} = 10$ s have slightly higher J_{SC} and V_{OC} than those with $t_{AS} = 30$ s. For the $X_{sol} = 0.6$, the opposite can be observed and it looks like for this mix the later 30 s timing could be preferable.

For the $X_{sol} = 0.7$ mix, the functioning devices for $t_{AS} > 10$ s are too few to make a comparison between timings in terms of device performance. As can be seen in Fig. S12 in SI:5, there are in total 18 devices (3 samples) fabricated for $t_{AS} = 10$ s and for $t_{AS} > 10$ s respectively. Among these, the 10 s timing produced 78% functioning devices while the the $t_{AS} > 10$ s samples only resulted in 11% functioning devices. This could mean that for the shorter timing it is more likely for a higher quality perovskite film to form, leading to functioning devices. This would be in agreement with the film quality seen in the SEM images. It may be that the poorer film quality for the 30 s and 55 s AS timings can be translated to a lower film quality also on device level with lower average performance and lower yield of functioning devices. The same reasoning cannot be applied on the 100% iodide devices based on these results, since in this case there was only one single sample fabricated with $t_{AS} < 30$ s.

Overall it looks like an early AS drop can be favorable for perovskites with high bromide content where the perovskite phase is formed directly. For the halide ratios with more iodide, for which we suspect that a solvate phase first forms (alone or simultaneously as a perovskite phase) based on the results from Rehermann et al. [17], the results are inconsistent. This could be due to more complicated interactions with the AS when the film formation path involves more steps.

J_{SC} and V_{OC} for different AS drip times

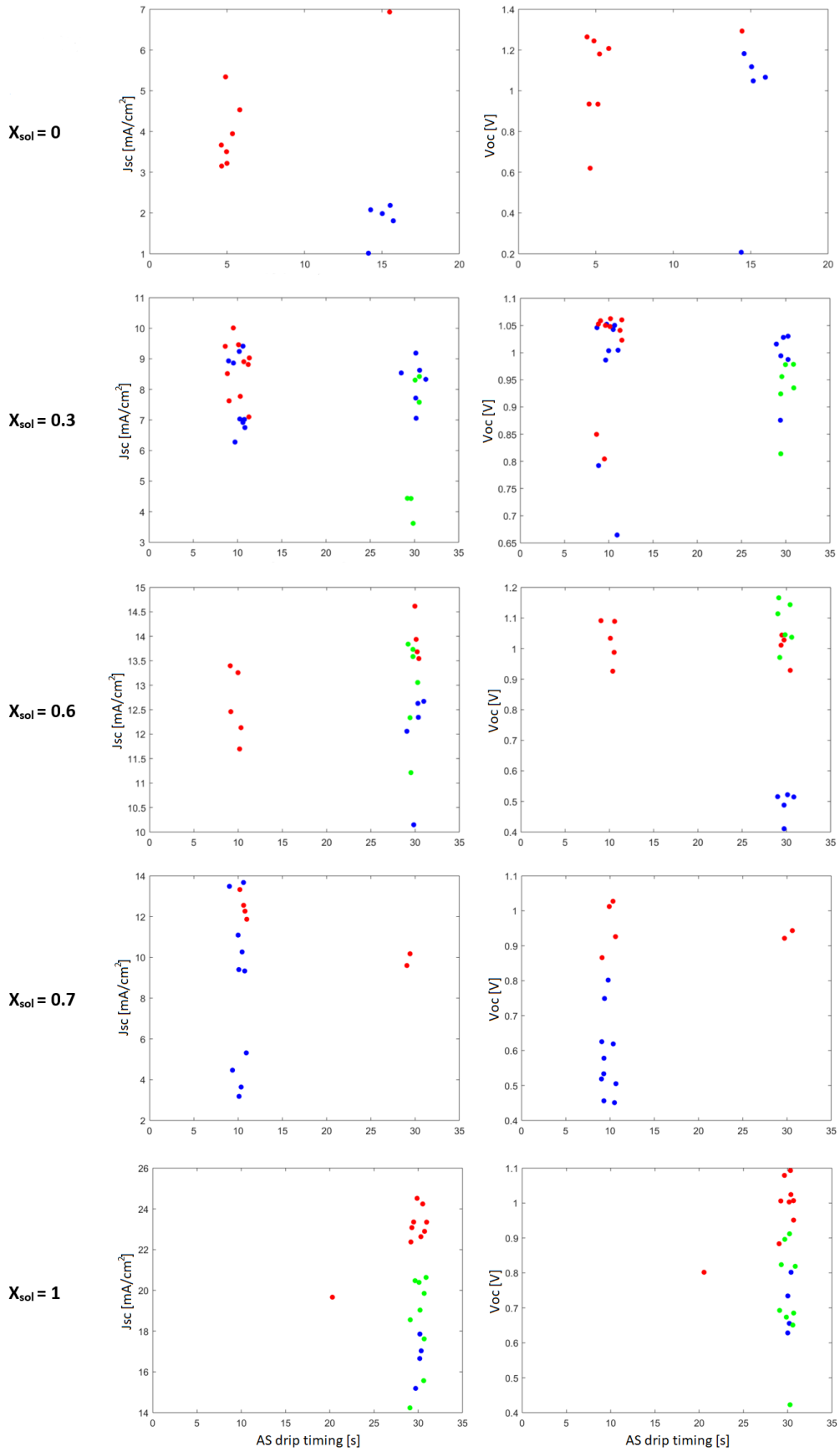


Figure 4.5: Device performance in terms of J_{SC} (left) and V_{OC} (right) for different AS drip times for each halide mix, $X_{sol} = 0, 0.3, 0.6, 0.7$ and 1 . Batches are differentiated by color.

4.2 Device behaviour for varying halide compositions

The plots in this section, seen in Fig. 4.6 and Fig. 4.7, are based on the same solar cells from batch 1-3 as were presented in the previous section. The plots only include the results of those devices that I have assessed to have an acceptable JV-behaviour and only those made with standard device layout, without any IM. In the boxplots the devices of each halide ratio are presented together regardless of batch or AS drip time, but they are differentiated by JV-scan direction. In the plots to the right, the same devices are plotted individually, each plotted data point represent the mean value of the forward and reverse JV-scan of that particular device. Batch numbers are there differentiated by color where the first, second and third batch are plotted in blue, red, and green respectively.

While the expected pattern is that the V_{OC} will decrease with an increasing ratio of iodide, as the V_{OC} is related to the bandgap, the results do not show consistency in this regard. It is especially noteworthy that the 60% iodide samples have a slightly higher median V_{OC} compared to the 30% iodide sample. In general the 60% mix samples show comparatively good performance. This could be related to high film quality. Although the SEM images from the previous section show some defects and morphological inhomogeneity, the result is very consistent with the images on device level presented in the next chapter, where the 60% mix sample has a lower film hole ratio compared to other halide mixes. This could be an explanation of the relatively high performance of the devices of this mix compared to the other mixed samples. In comparison to the 60% mix, it should be noted that especially devices from the third batch show high performance, while for the 70% mix, there are no devices from the third batch and if only devices from batch 1-2 were included, the difference in performance would be smaller. The double-pathway crystallization process where both a perovskite phase and an intermediate solvate phase are formed simultaneously, expected in the 30 and 60% iodide samples based on the results in the Rehermann et al. study [17], could lead to greater ionic inhomogeneity which in turn would lead to reduced V_{OC} , but this can not be detected on device level, rather it is the 70% sample that shows a comparatively low voltage.

The current density generally shows an expected pattern with higher iodide content leading to a higher J_{SC} , except for the 70% mix which shows a lower current compared to the 60% mix. It is worth to note that the 60% mix generally has a negative hysteresis index, and excluding the third batch which is not scanned in the same direction order as the first and second, this is especially apparent. The deviating hysteresis behaviour is however likely non-generalizable since this result mainly stems from unreasonably negative HI on a single sample from the first batch. Excluding this single sample, the HI behaviour is similar to that of the 30% mix. It is important to remember that the different scan direction order used for batch 1-2 and batch 3 respectively, means that especially hysteresis index can not be fairly compared between the batches.

Overall what stands out from the results is the generally low performance of the 70% devices. This could be due to poor film quality, however from the SEM images

in this chapter as well as the cross sectional SEM images in the next section, the 70% mix does not seem to result in worse film quality than many of the other mixes. Due to the few 70% devices characterized, we cannot statistically verify that the performance is lower for this mix.

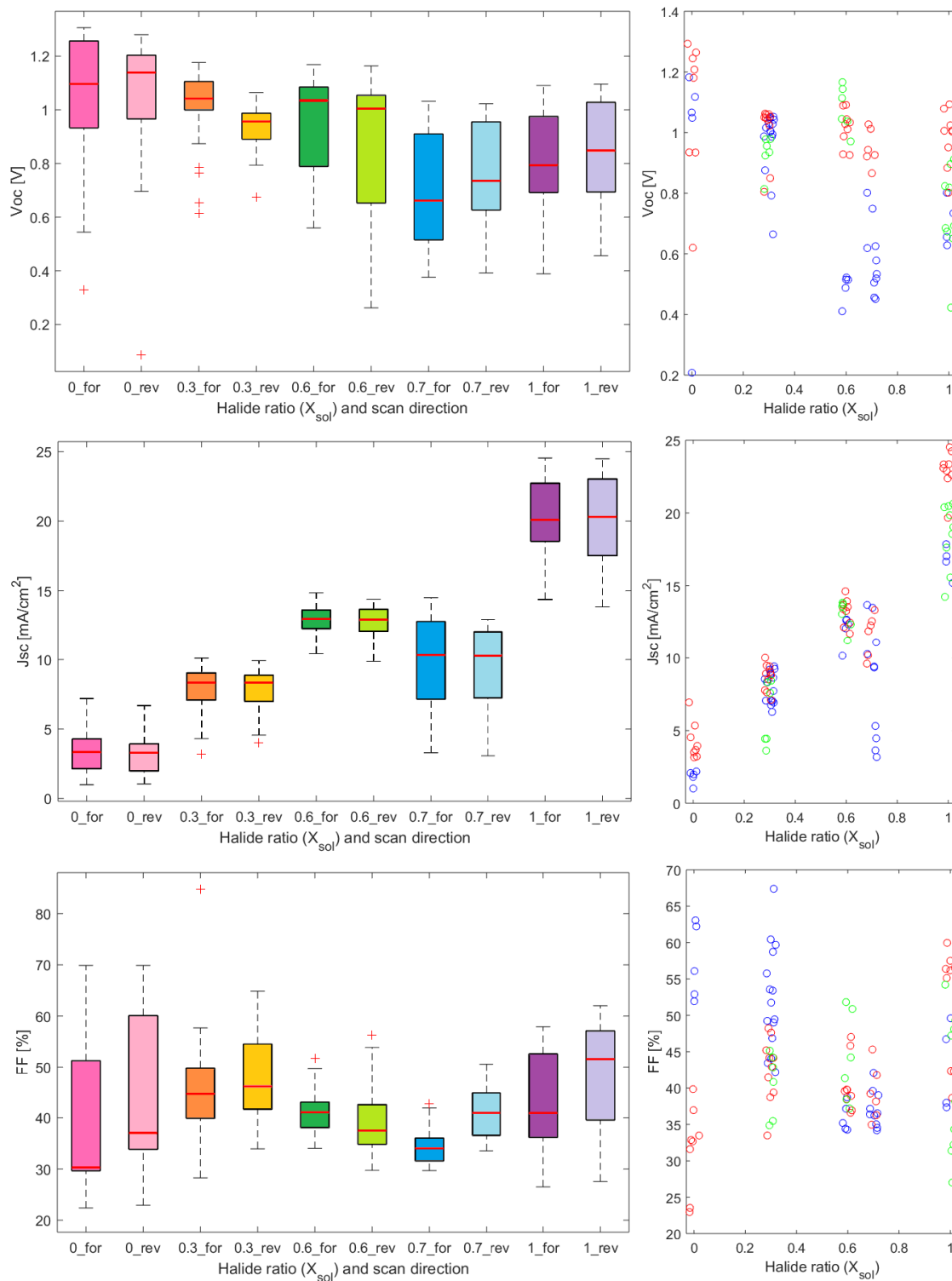


Figure 4.6: Device performance for each halide ratio, left images showing statistical plots with forward and reverse scan direction differentiated and the right images showing the same data with single devices plotted, colors showing the three batches included. The plots show V_{OC} , J_{SC} and FF from top to bottom.

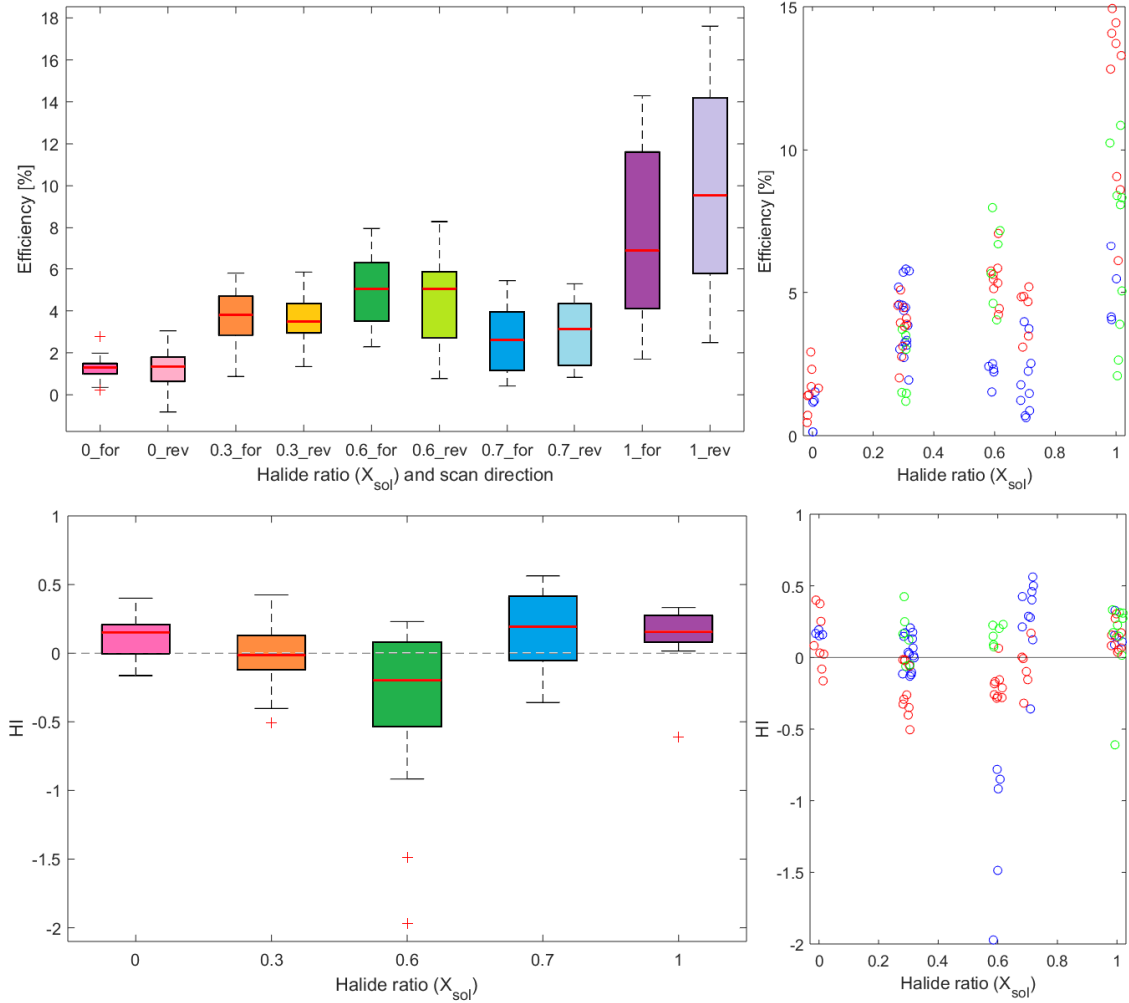


Figure 4.7: Device performance for each halide ratio, left images showing statistical plots with forward and reverse scan direction differentiated and the right images showing the same data with single devices plotted, colors showing the three batches included. The upper plots show PCE and the plots beneath show HI.

4.3 Interface modifiers

In the second study of the project we used IMs between the SnO_2 contact layer and the perovskite layer in order to see what impact it had on film quality and device performance for perovskites with different halide ratios. In this part, 80% iodide was used instead of 70% in order to achieve a more even spread of mixes.

Initially three different alkali salts were tried as IMs, KNO_3 in the third SC batch and KCl and NaCl in the fourth batch. As there are no SEM images of the fourth batch and the device level performance seemed to be the same or worse with these modifiers, the results presented only include the third batch where samples were made either with KNO_3 as IM or without any IM.

4.3.1 Film quality (SEM)

SEM images with a side view of the solar cell samples from batch 3, see Fig. 4.8, show the resulting film quality with and without KNO_3 as IM for each halide mix.

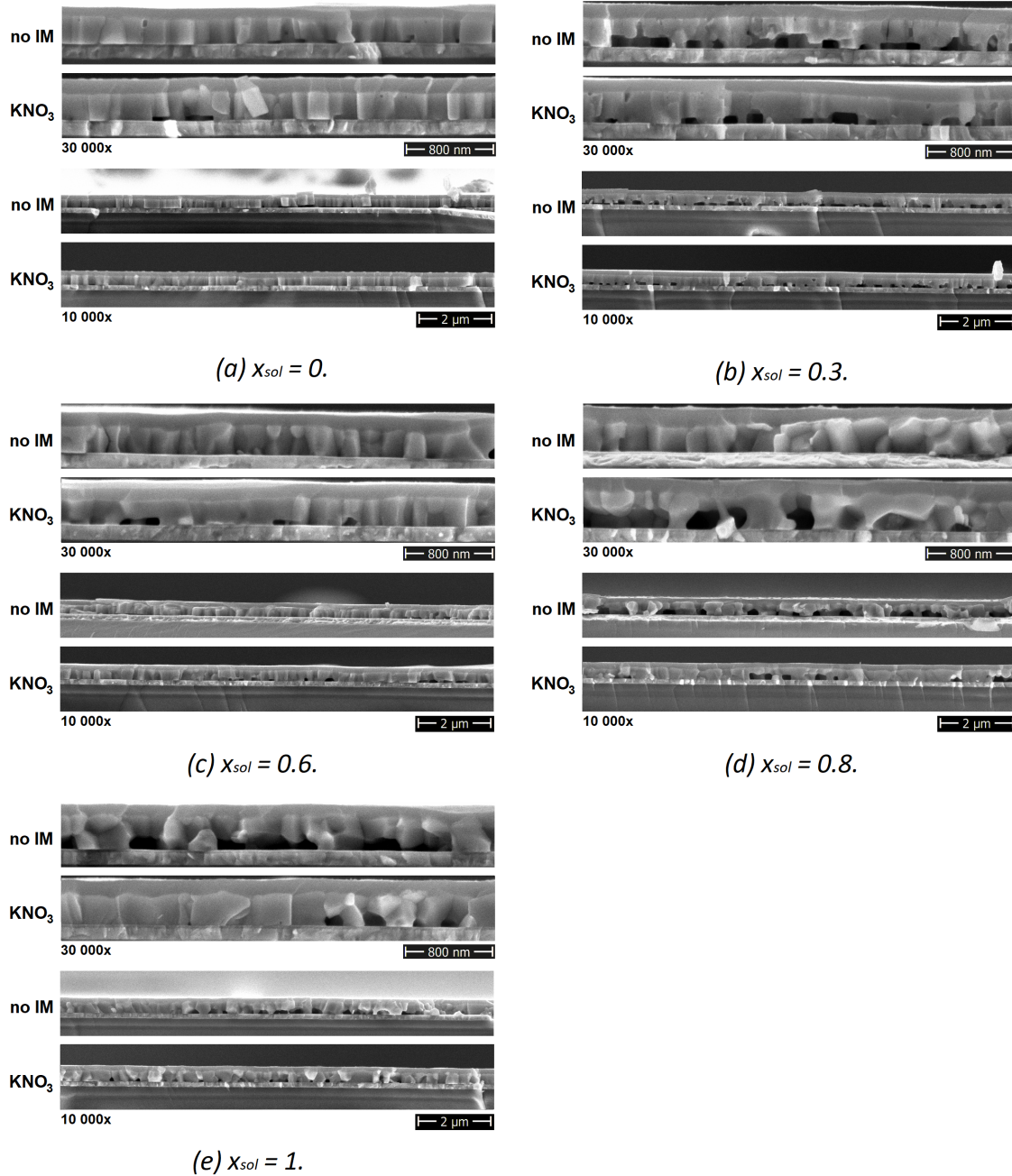


Figure 4.8: Cross sectional SEM images of SCs with and without KNO_3 as IM for each halide mix. Two images with different magnifying levels are included for each solar cell.

From these images the hole fraction of the perovskite film was estimated by measuring the added distance of holes in the perovskite film just above the contact layer below, i.e. the distance where the perovskite film visibly is not in contact with the contact layer. The hole fraction on the image was squared to obtain an estimate of hole fraction per area. For each studied sample there are two images, one with magnifying level of 10,000x and one with 30,000x. Since the two images do not overlap, the hole fraction estimates from each of them are considered as separate data

sets which are combined to obtain the best hole fraction estimate for the sample, as presented in Fig 4.9. To give equal consideration per length unit of the sample, the estimated value from the images with 10,000x magnifying level are valued three times higher in the calculation of the combined estimates. From the estimated hole fractions from the two images of each sample, which can be seen in SI:6, Fig. S14, it is clear that the overall film quality of a sample cannot be accurately estimated from a single image since the estimation differs greatly between the two images. The holes of the films are evidently too unevenly distributed in order for one image to accurately represent the overall film quality and hole fraction of the sample. Since combining the two available images only gives slightly better statistics of the films, the combined estimates can also not be assumed to accurately represent the film as a whole.

For the pure bromide perovskite as well as the 60% iodide mix it seems like the hole fraction will be quite low independently of IM, while the 30% and 80% mixes have a higher hole fraction. However, the combined estimate shows that the hole fractions of the samples where KNO_3 is used as an IM are lower for all mixes except 60%, where the hole fraction is very low for both samples. The results from this study are not reliable enough to conclude the influence of an KNO_3 IM, as evident from the inconsistency in estimated hole fraction between the two SEM images of each of the samples, but the estimation suggests that the IM can improve film quality by reducing the hole fraction of the film for either some or all halide mixes.

From the results it also seems like some halide mixes, especially 30% iodide, are more likely to form perovskite films in poor contact with the underlying layer while the 60% mix seem to easily form perovskites in good contact with the underlying layer. The clear difference between these two mixes is especially interesting since they are expected to take similar film formation routes according to the results in the Rehmann et al. [17] study.

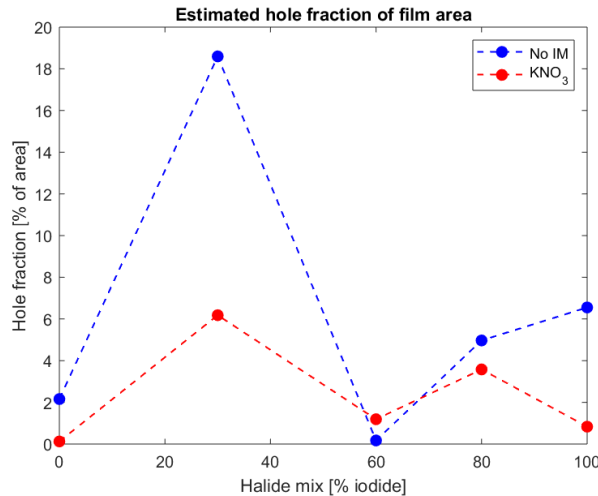


Figure 4.9: Hole fraction of film area at interface estimated from cross sectional SEM images of devices with halide ratios of $X_{sol} = 0, 0.3, 0.6, 0.8$ and 1. The blue dots represent devices with no IM and the red dots represent devices with KNO_3 used as an IM.

4.3.2 Device performance

In batch 3 and 4 with solar cells, devices were fabricated using either no IM or with KNO_3 , KCl or NaCl as IM. The iodide ratios used were $X_{sol} = 0, 0.3, 0.6, 0.8$ and 1. The results presented in this section are also based only on those devices I estimated to have a reasonable JV-behaviour. In the batches presented in this chapter, SCB3-4, we did not manage to produce any functional devices with pure bromide perovskite without any IM. For this single case, the result presented in the plots are based on the devices from batch 1-2.

For the open circuit voltage, the median value of the devices with KNO_3 used as an IM is higher for all halide mixes as compared to the median value for devices fabricated without the use of an IM. In all cases except for the 60% iodide mix, devices with this IM also had a higher V_{OC} than the devices with the other tested IMs. KNO_3 being the preferred IM is consistent with previous results [1]. The higher V_{OC} for devices with KNO_3 can be related to the higher film quality suggested from the results of the SEM images.

As we can see, it is only for the open circuit voltage that we observe a consistent behaviour with respect to the use of an IM and performance for the different halide ratios. For most of the halide ratios in batch 3-4, the results are mixed regarding performance parameters and IMs. However for the pure iodide mix, the devices fabricated using KNO_3 seem to perform better in all parameters studied as compared to devices without IM. As seen in figure 4.11 and 4.10, devices with KNO_3 have a higher efficiency, J_{SC} , V_{OC} and FF, and a lower hysteresis index compared to the devices without IM.

Comparing the results of the devices with the film quality based on the hole fraction estimates in Fig. 4.9, there seems to be a slight correlation between device performance and a higher film coverage, where the IM case which gave a higher coverage is the same that leads to a higher device efficiency for all halide ratios except for the 80% iodide mix.

These results suggest that using KNO_3 as an IM is beneficial for overall device performance for devices with pure iodide perovskites, which is in line with the results in the Dagar et al. [1] study. The perovskites used in that study had a high iodide content, the pure iodide mix in this project being the closest in composition. Since the results regarding which IM, if any, that leads to the best performance regarding efficiency, J_{SC} , V_{OC} , FF and HI are mixed for the other halide ratios, it seems like the beneficial effect that KNO_3 has on the pure iodide perovskite devices, cannot be translated to all perovskite mixes. Regarding the other halide ratios, which IM, if any, that most benefits device performance cannot be concluded from the results of this study, although it seems that a KNO_3 treatment of the interface is beneficial for V_{OC} for all halide ratios. Further studies are needed to confirm that the benefit of adding KNO_3 depends on halide ratio, and if this is the case, to find out the cause of this difference.

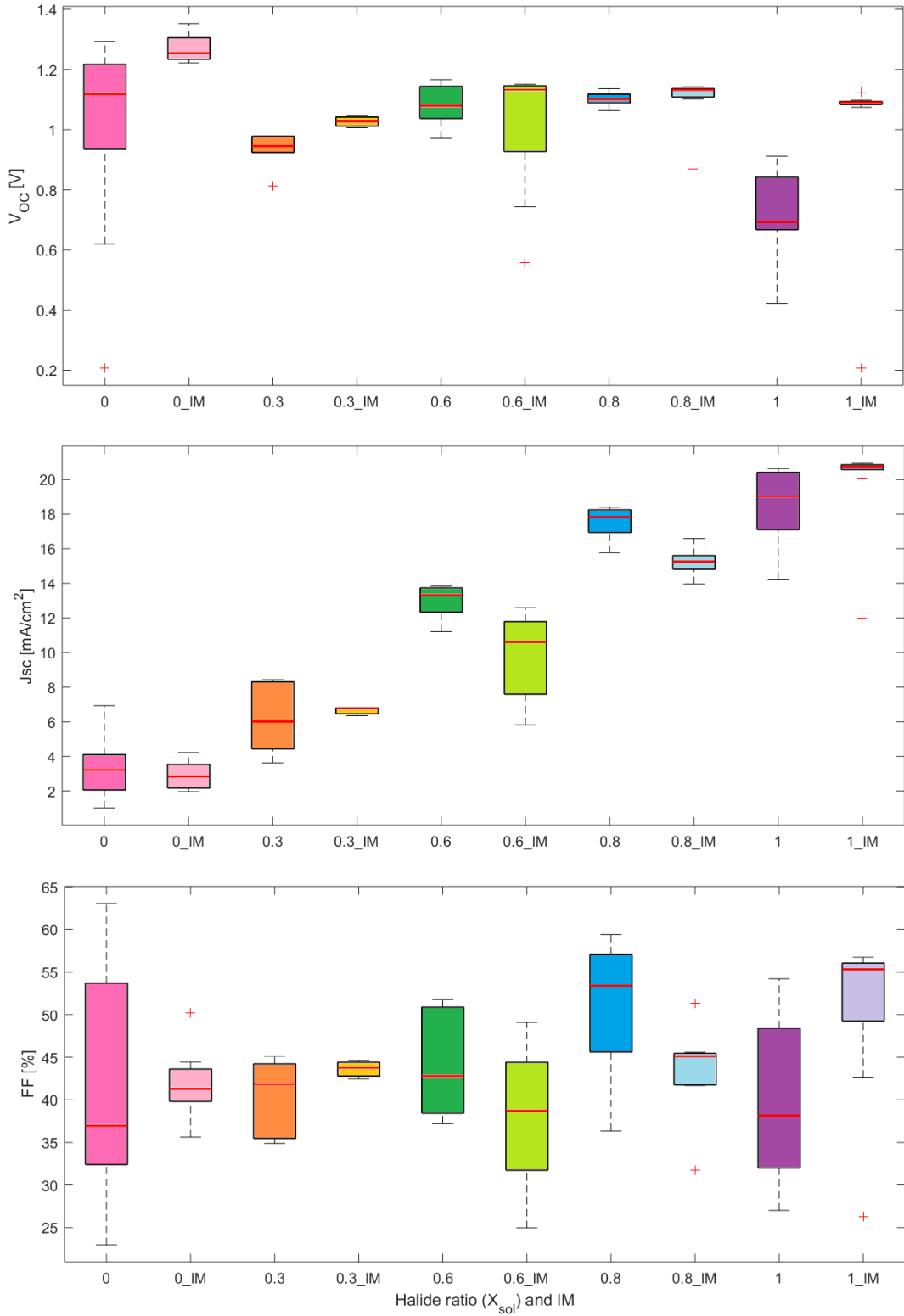


Figure 4.10: Statistical plots of V_{OC} , J_{SC} and FF for devices with and without KNO_3 as IM for each halide ratio.

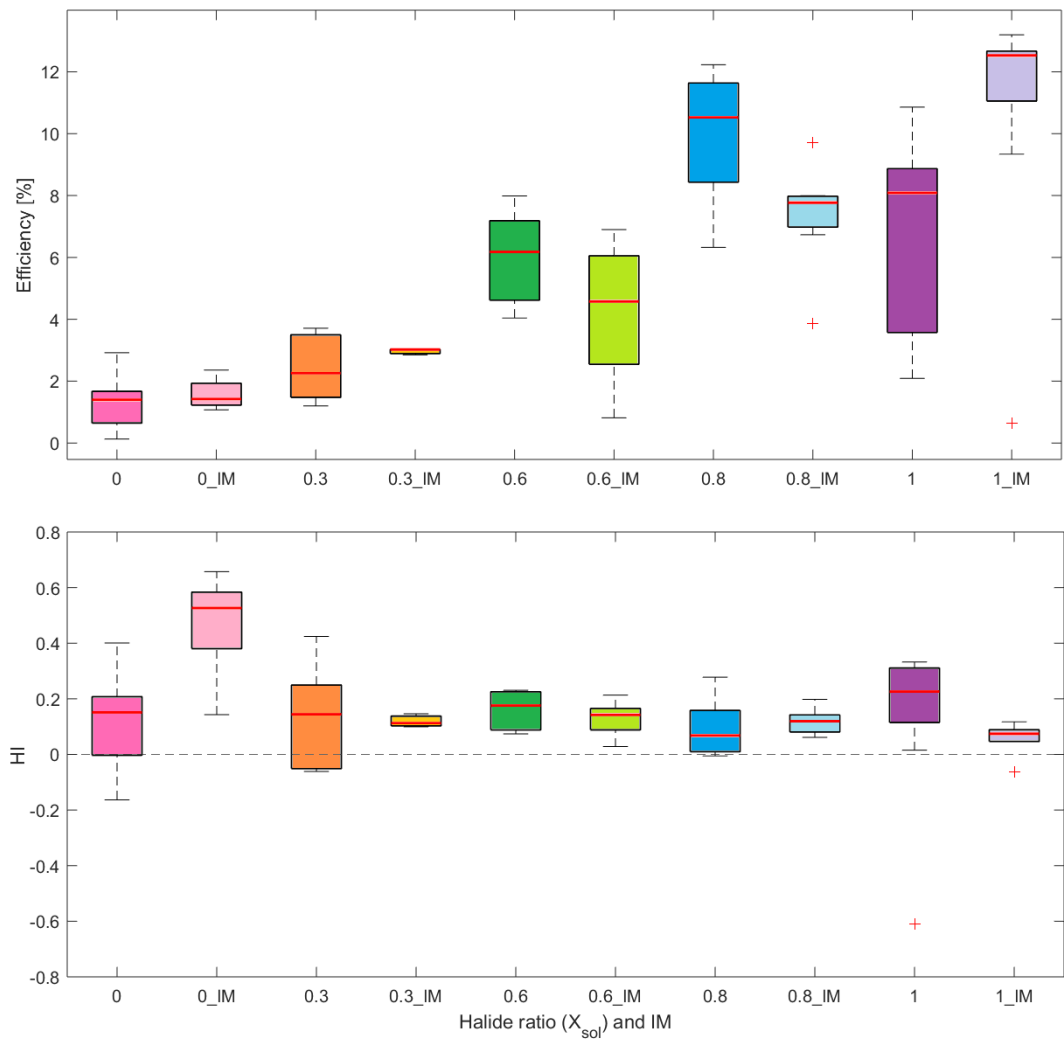


Figure 4.11: Statistical plots of PCE (upper plot) and HI (lower plot) for devices with and without KNO_3 as IM for each halide ratio.

4.4 Discussion on methods

Within the scope of this master's thesis project, many experiments were carried out during a time period of just a few weeks. This has many advantages in terms of personal learning, as I learned about many more characterization methods etc. than the few that got included in the report. The drawback is that there was limited possibilities to adapt the upcoming experiments to previous results or lack thereof. The result of this is firstly that only a few of the performed experiments could be part of the report. Secondly, few if any of the results from the experiments are based on data that are sufficient both in terms of quality and quantity that conclusions can be drawn with high certainty. Instead, all results need to be considered only as guidance or hints for future, more thorough, experimental investigations.

In the data from the JV-measurements, which constitute a large part of the measurements that have been analyzed and presented, the noise in the data, caused mainly by low quality of the devices, was too high to detect any patterns that depend on the studied parameters. Due to this, some of the noise had to be removed in order to receive any valuable results.

In lack of more objective methods to evaluate the quality of each data point included, this was done by visually assessing each JV-curve and how far it deviates from the expected characteristic solar cell behavior where too much deviation meant that the device was removed from the presented data. Details about how this was carried out can be seen in SI:4. Since the resulting performance parameters can take any value, low or high, for "broken" solar cells with deviating JV-behaviour, it is not enough to sort them based on the values of these parameters. The lack of objectivity in this manual sorting process adds to the uncertainty of the results. A method to do the sorting automatically or with fixed, quantitatively based criteria would have helped to increase the credibility of the presented results.

5

Conclusions

The results from this project do in several cases suggest some patterns regarding how film quality and device performance may be related to halide ratio and film formation conditions such as AS treatment and the underlying surface. Some of these observations as well as suggestions for further research are presented below.

5.1 Empirical observations

Film formation with antisolvent

- AS treatment seems to be beneficial for formation of perovskite films with high coverage. This could be observed from both the in-situ experiments as well as from the SEM images of resulting films. A likely explanation is that an AS drop helps the formation of seed crystals at an early stage of the drying process which helps the formation of a closed, homogeneous film.
- The timing of the AS drop seem to have some influence on the resulting film as well as on device performance. Since the differences in results between AS timings for the same halide mix from the experiments both on film and device level are so slight, this effect is probably not overwhelmingly large, but can be important to consider for high performance devices.
- Which AS timing that leads to the highest film quality and highest device performance seems to be dependent on the halide mix and is not obvious from the results. It seems like perovskites with high bromide content benefit from an early AS drop while the results vary for perovskites with higher iodide content. The inconclusiveness of these results can be due to the fact that the interactions between the AS and the precursor solution are more complex with the formation of a solvate phase involved.
- The high iodide mixes with $\geq 70\%$ that do not form a perovskite phase when spin coated without AS treatment according to the Rehermann et al. [17] study also do not form a perovskite phase during spin coating when treated with AS. Since the AS removes solvents from the ions forming the perovskite, it could be argued that AS treatment would prevent the formation of the solvate phase, but it seems that also with AS treatment the formation of the solvate phase during spin coating is still the most thermodynamically beneficial for

high iodide compositions. AS treatment seems to be beneficial for the film quality also for these mixes where initially only a solvate phase is formed.

- When an AS drop is set around the natural crystallization onset of the perovskite precursor solution, the crystallization process is more rapid as compared to a non treated sample.
- In most of the cases in the in-situ UV-vis experiment the AS induces crystallization immediately after being dripped on the sample during spin coating, however; a couple of exceptions could be found. It is not clear from the results if it is important for film quality that the AS induces crystallization directly, to answer this further experiments are needed. Studying this further could reveal if there is an earliest AS timing for each of the ionic compositions that results in immediate crystallization and how this is, if at all, related to the natural crystallization onset of the ionic composition, the competing formation pathways of the perovskite, and to the type of AS.
- The underlying surface that the perovskite is spin coated onto seems to influence the film formation and the effect seems to be halide ratio depend. In general, the difference in film quality between the samples with and without AS treatment is smaller for the samples spin coated on SnO_2 . This suggests that the results from experiments of film formation on plain glass substrate can not be directly translated to results on device level where the perovskite is spin coated on other layers of the device.

Device performance related to halide composition

- When comparing device performance between perovskites with different halide ratios, the experiments show better performance for the 60% iodide perovskite mix as compared to the 70% iodide mix. Further experiments including a larger number of tested devices would be needed to statistically verify a higher performance of devices with the 60% as compared to the 70% iodide mix. Including more iodide to bromide ratios would be needed to confirm if this is related to differences in crystallization pathways where AS treatment potentially is more beneficial when a perovskite phase forms during spin coating.
- For devices with the 30% and 60% iodide mixes that are expected to form via two simultaneous crystallization pathways, possibly leading to ionic inhomogeneity that promotes Hoke effect, there is no sign of a lower V_{OC} . Rather it is the 70% mix that shows a comparatively low V_{OC} . What can be observed comparing the batches within the 60% iodide mix, is that the devices with the highest absolute value of HI, indicating lower stability, are also the devices with the lowest V_{OC} .

Interface modifiers

- Using KNO_3 as an IM seems to lead to a higher ratio of contact between the perovskite layer and the underlying transport layer for the $\text{MAPb}(\text{I}_x, \text{Br}_{1-x})_3$ perovskite series by reducing the amount of holes in the film at the interface.

- It seems to be a clear difference in layer contact ratio between perovskites depending on halide mix, regardless of IM.
- On a device level, KNO_3 as IM seem to improve V_{OC} compared to using no IM. For other performance parameters, the results vary.
- For the pure iodide perovskite, KNO_3 as IM seems to be beneficial compared to using no IM regarding all performance parameters (V_{OC} , J_{SC} , FF, PCE and HI). Since there is no clear difference in overall performance for the other halide ratios investigated, this suggests that the benefit of a specific IM might be dependent on which ionic composition of the perovskite that is used.

5.2 Future prospects

Further studying the film formation conditions for mixed halide perovskites could give many valuable insights for the development of highly efficient perovskite solar cells with improved stability under operating conditions. Many of the experiments within this project could be further developed to contribute to this development. Following are a few examples of what I would suggest to study further based on insights from this project.

- Investigating the influence of AS timing on device level with cross sectional SEM imaging as was used to study the influence of IM in this project.
- Developing the first experiment with in-situ UV-vis using a range of AS drip times to find out which is the most beneficial for a particular halide mix and further investigating the conditions for immediate crystallization onset after AS is dripped.
- Using in-situ UV-vis tracking to see how the annealing process might be different after AS treatment compared to for non-treated samples to give further insights into how AS treatment affects the film formation process.
- Studying the effect of KNO_3 on high iodide perovskites using several halide mixes with high iodide content to see how the benefits of the IM possibly are related to iodide content.

References

- [1] J. Dagar, K. Hirselandt, A. Merdasa, A. Czudek, R. Munir, F. Zu, N. Koch, T. Dittrich, and E. L. Unger, “Alkali salts as interface modifiers in n-i-p hybrid perovskite solar cells,” *Sol. RRL*, vol. 3, no. 1900088, 2019. DOI: [10.1002/solr.201900088](https://doi.org/10.1002/solr.201900088).
- [2] A. Smets, K. Jäger, O. Isabella, R. Van Swaaij, and M. Zeman, *Solar Energy - The physics and engineering of photovoltaic conversion, technologies and systems*. UIT Cambridge Ltd, 2016, ISBN: 9781906860325.
- [3] P. Würfel and U. Würfel, *Physics of Solar Cells - From Basic Principles to Advanced Concepts*, 3rd ed. Wiley-VCH, 2016, pp. 41–169, ISBN: 9783527413126.
- [4] E. L. Unger, L. Kegelmann, K. Suchan, D. Sörell, L. Korte, and S. Albrecht, “Roadmap and roadblocks for the band gap tunability of metal halide perovskites,” *J. Mater. Chem. A*, vol. 5, pp. 11 401–11 409, 2017. DOI: [10.1039/c7ta00404d](https://doi.org/10.1039/c7ta00404d).
- [5] Z. Song, C. Chen, C. Li, R. A. Awni, D. Zhao, and Y. Yan, “Wide-bandgap, low-bandgap, and tandem perovskite solar cells,” *Semicond. Sci. Technol.*, vol. 34, no. 093001, 2019. DOI: [10.1088/1361-6641/ab27f7](https://doi.org/10.1088/1361-6641/ab27f7).
- [6] J. H. Noh, S. H. Im, J. H. Heo, T. N. Mandal, and S. I. Seok, “Chemical management for colorful, efficient, and stable inorganic organic hybrid nanostructured solar cells,” *Nano Letters*, vol. 13, pp. 1764–1769, 2013. DOI: [10.1021/nl400349b](https://doi.org/10.1021/nl400349b).
- [7] E. T. Hoke, D. J. Slotcavage, E. R. Dohner, A. R. Bowring, H. I. Karunadasa, and M. D. McGehee, “Reversible photo-induced trap formation in mixed-halide hybrid perovskites for photovoltaics,” *Chemical Science*, vol. 6, pp. 613–617, 2015. DOI: [10.1039/c4sc03141e](https://doi.org/10.1039/c4sc03141e).
- [8] N. J. Jeon, J. H. Noh, W. S. Yang, Y. C. Kim, S. Ryu, J. Seo, and S. I. Seok, “Compositional engineering of perovskite materials for high-performance solar cells,” *Nature*, vol. 517, pp. 476–480, 2015. DOI: [10.1038/nature14133](https://doi.org/10.1038/nature14133).
- [9] T. J. Jacobsson, “Temperature effects in lead halide perovskites,” in *Characterization Techniques for Perovskite Solar Cell Materials*, M. Pazoki, A. Hagfeldt, and T. Edvinsson, Eds., Elsevier, 2019, pp. 197–215, ISBN: 9780128147283.
- [10] N. Phung and A. Abate, “Stability of materials and complete devices,” in *Characterization Techniques for Perovskite Solar Cell Materials*, M. Pazoki, A. Hagfeldt, and T. Edvinsson, Eds., Elsevier, 2019, pp. 197–215, ISBN: 9780128147283.

- [11] T. Leijtens, K. A. Bush, R. Prasanna, and M. D. McGehee, “Opportunities and challenges for tandem solar cells using metal halide perovskite semiconductors,” *Nature Energy*, vol. 3, no. 10, pp. 828–838, 2018. DOI: [10.1038/s41560-018-0190-4](https://doi.org/10.1038/s41560-018-0190-4).
- [12] NREL. (). “Best research-cell efficiency chart,” [Online]. Available: <https://www.nrel.gov/pv/cell-efficiency.html>. (accessed: 11.08.2020).
- [13] A. Sadhanala, F. Deschler, T. H. Thomas, S. E. Dutton, K. C. Goedel, F. C. Hanusch, M. L. Lai, U. Steiner, T. Bein, P. Docampo, D. Cahen, and R. H. Friend, “Preparation of single-phase films of $\text{CH}_3\text{NH}_3\text{Pb}(\text{I-xBr}_x)_3$ with sharp optical band edges,” *J.Phys.Chem.Lett.*, vol. 5, pp. 2501–2505, 2014. DOI: [10.1021/jz501332v](https://doi.org/10.1021/jz501332v).
- [14] E. L. Unger, E. T. Hoke, C. D. Bailie, W. H. Nguyen, A. R. Bowring, T. Heumüller, M. G. Christoforod, and M. D. McGehee, “Hysteresis and transient behavior in current–voltage measurements of hybrid-perovskite absorber solar cells,” *Energy Environ. Sci.*, vol. 7, pp. 3690–3698, 2014. DOI: [10.1039/c4ee02465f](https://doi.org/10.1039/c4ee02465f).
- [15] Z. Wang, D. P. McMeekin, N. Sakai, S. van Reenen, K. Wojciechowski, J. B. Patel, M. B. Johnston, and H. J. Snaith, “Efficient and air-stable mixed-cation lead mixed-halide perovskite solar cells with n-doped organic electron extraction layers,” *Adv. Mater.*, vol. 29, no. 1604186, 2017. DOI: [10.1002/adma.201604186](https://doi.org/10.1002/adma.201604186).
- [16] L. Kegelmann, C. M. Wolff, C. Awino, F. Lang, E. L. Unger, L. Korte, T. Ditttrich, D. Neher, B. Rech, and S. Albrecht, “It takes two to tango- double-layer selective contacts in perovskite solar cells for improved device performance and reduced hysteresis,” *ACS Appl. Mater. Interfaces*, vol. 9, pp. 17245–17255, 2017. DOI: [10.1021/acsami.7b00900](https://doi.org/10.1021/acsami.7b00900).
- [17] C. Rehmann, A. Merdasa, K. Suchan, V. Schröder, F. Mathies, and E. L. Unger, “Origin of ionic inhomogeneity in $\text{MAPb}(\text{I-xBr}_x)_3$ perovskite thin films revealed by in-situ spectroscopy during spin coating and annealing,” *ACS Applied Materials Interfaces*, vol. 12, pp. 30343–30352, 2020. DOI: [10.1021/acsami.0c05894](https://doi.org/10.1021/acsami.0c05894).
- [18] M. M. Tavakoli, P. Yadav, D. Prochowicz, M. Sponseller, A. Osherov, V. Bulovic, and J. Kong, “Controllable perovskite crystallization via antisolvent technique using chloride additives for highly efficient planar perovskite solar cells,” *Adv. Energy Mater.*, vol. 9, no. 1803587, 2019. DOI: [10.1002/aenm.201803587](https://doi.org/10.1002/aenm.201803587).
- [19] S. Paek, P. Schouwink, E. N. Athanasopoulou, K. T. Cho, G. Grancini, Y. Lee, Y. Zhang, F. Stellacci, M. K. Nazeeruddin, and P. Gao, “From nano- to micrometer scale: The role of antisolvent treatment on high performance perovskite solar cells,” *Chem. Mater.*, vol. 29, pp. 3490–3498, 2017. DOI: [10.1021/acs.chemmater.6b05353](https://doi.org/10.1021/acs.chemmater.6b05353).

- [20] M. Abdi-Jalebi, Z. Andaji-Garmaroudi, S. Cacovich, C. Stavrakas, B. Philippe, J. M. Richter, M. Alsari, E. P. Booker, E. M. Hutter, A. J. Pearson, S. Lilliu, T. J. Savenije, H. Rensmo, G. Divitini, C. Ducati, R. H. Friend, and S. D. Stranks, “Maximizing and stabilizing luminescence from halide perovskites with potassium passivation,” *Nature*, vol. 555, pp. 497–501, 2018. DOI: [10.1038/nature25989](https://doi.org/10.1038/nature25989).
- [21] L. Tan, A. Tang, Y. Zou, M. Long, Y. Zhang, J. Ouyang, and J. Chen, “Sb₂Se₃ assembling sb₂O₃@ attapulgite as an emerging composites for catalytic hydrogenation of p-nitrophenol,” *Sci. Rep.*, vol. 7, no. 3281, 2017. DOI: [10.1038/s41598-017-03281-z](https://doi.org/10.1038/s41598-017-03281-z).
- [22] C. Rehermann, “Exploring the precursor-process-property space in metal halide perovskite thin films,” Ph.D. dissertation, Humboldt-Universität, 2020.